Energy Localization in Molecules, Bifurcation Phenomena, and Their Spectroscopic Signatures: The Global View

Stavros C. Farantos,*,† Reinhard Schinke,‡ Hua Guo,§ and Marc Joyeux||

Institute of Electronic Structure and Laser, Foundation for Research and Technology—Hellas, and Department of Chemistry, University of Crete, Iraklion 711 10, Crete, Greece, Max-Planck-Institut für Dynamik und Selbstorganisation, D-37073 Göttingen, Germany, Department of Chemistry and Chemical Biology, University of New Mexico, Albuquerque, New Mexico 87131, and Laboratoire de Spectrométrie Physique, Université Joseph Fourier—Grenoble I, BP 87, F-38402, St. Martin d'Heres Cedex, France

Received February 20, 2009

Contents

1. Introduction 4248
2. Global and Spectroscopic Hamiltonians 4251
3. Quantum and Semiclassical Vibrational Eigenstates 4252
4. Elementary Bifurcations of Equilibria and Periodic Orbits 4254
   4.1. Model Hamiltonians 4254
   4.2. Periodic Orbits 4256
5. Triatomic Molecules 4258
   5.1. Methylene 4259
   5.2. Ozone 4261
      5.2.1. Ground State $O_3(X^1A_2)$ 4261
      5.2.2. Excited State $O_3(1^1B_2)$ 4263
6. Polyatomic Molecules 4264
   6.1. Acetylene 4264
   6.2. Biomolecules 4266
7. Conclusions 4268
8. Acknowledgments 4268
9. References 4269

1. Introduction

Controlling chemical reactions by selecting specific bond or vibrational mode excited states of the reactants and analyzing the energy disposal into specific vibrational states as well as into rotational and translational degrees of freedom of the product molecules has been an ambitious project in chemical dynamics[1] for a long time. Deuterated methane is a good example for which it has been proved that vibrationally excited states control the course of the reaction with chlorine atoms.[2] Excitation of C−H or C−D overtone states promotes the formation of CH_2D or CH_3 product, respectively. Similarly, convincing evidence for the mode-selective desorption of H_2 from a hydrogen-covered silicon surface, Si(111), by using tunable infrared radiation has been found.[3,4] The wavelength dependence of the desorption yield peaks at 0.26 eV, the energy of the Si−H vibrational stretch mode. Such selectivities and specificities have been obtained thanks to the progress in experimental spectroscopic techniques[3,5] and molecular beams. However, this endeavor reveals the problems related to the assignment of the spectra of vibrationally excited molecules and the elucidation of the mechanisms for intramolecular vibrational energy redistribution (IVR), the solutions of which require a comprehensive understanding of molecular dynamics.

Generally, elementary chemical reactions, dissociation−recombination−isomerization, involve breaking and forming simple chemical bonds, and most often significant energy is required to overcome potential barriers. Thus, reacting molecules are vibrationally excited species, far from their equilibrium states, rendering the usual harmonic normal-mode analysis, valid at low excitation energies, inaccurate. The molecular potential energy surfaces (PESs) reveal the reaction paths, and they are generally nonlinear functions with strong couplings among the degrees of freedom which allow the energy to flow. For this reason, it is not surprising that the advances of nonlinear classical mechanics,[6,7] started with the pioneering work of Henry Poincaré[8] and mainly developed in the second half of the twentieth century, introduced new methods and concepts in the theories of vibrationally excited and reacting molecules. As found for general nonlinear dynamical systems with a few degrees of freedom, excited molecules are expected to show chaotic motions in which the energy is redistributed to many bonds, resonances, energy localization among specific bonds, and bifurcations of vibrational modes[9−11] to produce new type of motions as energy increases.

Nonlinear classical mechanics offer a systematic way to study complex systems. The hierarchical detailed exploration of the molecular *phase space structure* (Figure 1) requires first the location of the equilibrium points of the potential function and then the location of periodic orbits (POs) that emanate from the equilibrium points, the tori around stable POs, stable and unstable manifolds for the unstable POs, cantori,[12,13] and transition state objects such as the normally hyperbolic invariant manifolds (NHIM).[14−17] According to the scheme of Figure 1, periodic orbits can be considered as the first order approximation to the dynamics of the molecule, with the equilibria of the PES being the zero order approximation. We say that families of periodic orbits for a range of energies form the backbone of the phase space structure.

Do the classical nonlinear mechanical motions have quantum mechanical counterparts with spectroscopic fingerprints?

* Address for corresponding author: Institute of Electronic Structure and Laser, Foundation for Research and Technology-Hellas, Vasilika Vouton, Iraklion 71110, Crete, Greece. Telephone: +30 2810 391813. Fax: +30 2810 391305. E-mail: farantos@iesl.forth.gr.
† Institute of Electronic Structure and Laser, Foundation for Research and Technology—Hellas, and Department of Chemistry, University of Crete.
‡ Max-Planck-Institut für Dynamik und Selbstorganisation.
§ University of New Mexico.
|| Université Joseph Fourier—Grenoble I.

10.1021/cr900069m CCC: $71.50
Published on Web 07/06/2009

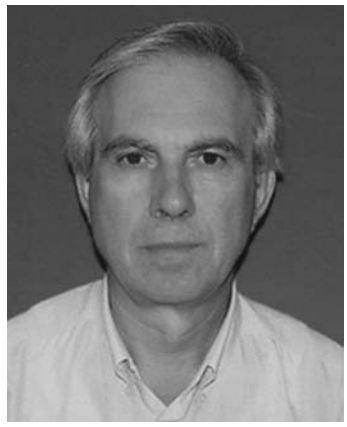

Stavros Farantos is Professor of Theoretical and Computational Chemistry at the University of Crete and a research scientist at the Institute of Electronic Structure and Laser of Foundation for Research and Technology—Hellas. His research interests are focused on theoretical vibrational spectroscopy of small polyatomic molecules with atmospheric interest, energy localization and redistribution in biological molecules, and spectroscopy, dynamics, and thermodynamics of atomic and molecular clusters. He has published more than 100 papers in refereed journals of chemical physics and physical chemistry. Currently, he is interested in the development of methods and computer codes for novel high performance computational schemes, such as grid computing, with applications in (semi)classical and quantum dynamics.

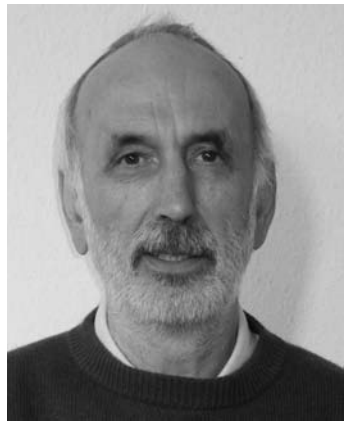

Reinhard Schinke is a Research Assistant at the Max-Planck Institut für Dynamik and Selbstorganisation in Göttingen. His research focuses on the theory of molecular dynamics, especially molecular collisions, vibrational spectroscopy, photodissociation, and the recombination of molecules. He has published more than 260 scientific articles in refereed journals, including several reviews. He is author of the book *Photodissociation Dynamics* (Cambridge University Press, 1993). In recent years he concentrated on the recombination and dissociation of ozone.

This question has given an impetus for the revival of semiclassical theory[18−20] which formulates the correspondence between quantum eigenfunctions and stationary classical mechanical objects such as tori and periodic orbits. At the same time, the development of spectroscopic techniques for investigating highly excited vibrational states of polyatomic molecules has put forward the need for assigning quantum states and extracting the dynamics. It turns out that the new spectroscopic methods provide the necessary high resolution, temporal and spatial, spectra to investigate the above question. Stimulated emission pumping (SEP), a double-resonance technique, and dispersed fluorescence (DF) spectroscopy[5] gave an impetus to the field of vibrationally excited molecules in the ground electronic state. Among the molecules studied by SEP and DF spectroscopy are C_2H_2,[21−27] HCP,[28] SO_2,[29−31] HFCO,[32,33] HCO,[34,35] DCO,[36] HCN,[37] NO_2,[38] and $SCCl_2$.[39]

Hua Guo is Professor of Chemistry at the University of New Mexico. He received his D.Phil. at Sussex University (U.K.) with John Murrell and worked as a postdoctoral fellow in the group of George Schatz at Northwestern University. His research interests include quantum mechanical characterization of highly excited vibrational states and of reaction dynamics, as well as computational enzymology. He is the author of about 190 publications.

Marc Joyeux is Chercheur CNRS at the Laboratoire de Spectrométrie Physique of Université Joseph Fourier—Grenoble 1. His research interests deal with the dynamics of molecular systems ranging from triatomic molecules to DNA models with several thousands degrees of freedom, which he studies with a panel of techniques including quantum mechanics, perturbation theory, semiclassical quantization, molecular dynamics simulations, and statistical physics. He has published over 60 papers in refereed journals.

Since SEP and DF methods excite the molecule at very high vibrational states, they are ideal to deduce the dynamics close to the isomerization or dissociation threshold. As a matter of fact, the SEP spectra of acetylene were the first which revealed vibrational (quantum) chaos at energies above the threshold for acetylene to vinylidene isomerization.[27] Vibrational overtone spectroscopy has experienced similar developments.[40] Crim and co-workers[41] have combined the photoacoustic spectroscopy with a time-of-flight apparatus to control the products in unimolecular and bimolecular reactions by vibrationally exciting specific chemical bonds of reactant molecules. This bond selective chemistry reveals energy localization in specific bonds.

Questions related to energy localization and transfer are currently put forward for biological molecules such as proteins.[42,43] Time resolved infrared and Raman spectroscopy spanning a time interval from femtoseconds[44−47] to milliseconds[48−50] is a major spectroscopic technique for studying the dynamics

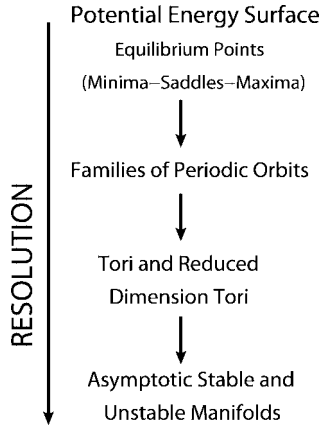

Figure 1. Invariant geometrical structures in the classical phase space of a molecule.

of biomolecules. Furthermore, efforts to find localized motions in infinite periodic or random anharmonic lattices have led to the concept of discrete breathers.[51,52] The initial theoretical observations of localized motions in the work of Sievers and Takeno[53] triggered the discovery of significant mathematical theorems for the existence of local stationary objects such as periodic orbits in infinite dimensional lattices.

Polyatomic molecules stimulate new computational challenges in accurately solving the Schrödinger equation and obtaining hundreds of vibrational states. Nowadays, triatomic molecules can be treated with fully *ab initio* methods, in both their electronic and nuclear parts. Tetratomic molecules are more difficult to deal with, in spite of the progress which has recently been achieved.[54] For example, six-dimensional calculations up to energies of the isomerization of acetylene to vinylidene have been published.[55]

The progress of nonlinear mechanics forces us to reexamine the mechanisms of breaking and/or forming of a single chemical bond as it occurs in elementary chemical reactions. New assignment schemes which allow the classification of quantum states in a meaningful and useful way are required, and such novel methods have been developed thanks to nonlinear mechanics and semiclassical theories for establishing a classical-quantum correspondence.[11,56−61] Most of the methods are based on spectroscopic Hamiltonians and their representations in action-angle variables.[62] Although they provide the means for assigning and extracting the dynamics of the majority of eigenstates in a polyad, they are limited to reduced dimensionality of two or three degrees of freedom. Another drawback is the loss of a direct contact with the physical coordinate space of the molecules (Cartesian), since the semiclassical quantization usually requires a perturbation expansion of the Hamiltonian in action-angle variables such as the Birkhoff−Gustavson one.[63−65]

On the other hand, periodic orbits[51,66,67] associated with *global* PESs, their bifurcations,[7,68] and semiclassical counterparts[19,69] are free of these limitations. As is demonstrated in the following sections, (i) POs can be located for polyatomic molecules with a large number of degrees of freedom and systematically studied with any type of potential functions and coordinates. (ii) They are easily visualized in a physical coordinate system, such as Cartesian, valence, or Jacobi coordinates. (iii) We can identify resonances among the vibrational modes, and thus, effective Hamiltonians can be constructed or a more general resonance map in phase space such as the Arnold web.[61,70,71] Direct comparison of quantum eigenfunctions with periodic orbits has revealed their localization along POs, stable as well as unstable[72] ones. For vibrationally highly excited molecules, a good correspondence between overtone states and periodic orbits has been determined for several molecules;[9−11,24] however, it is more difficult to establish a correspondence among combination states and POs.[73,74]

The landscape of the PES may be drastically altered as some parameters in the molecule vary.[75] Barriers and minima may disappear or appear. Similarly, the phase space changes with the total energy. Stable, quasiperiodic motions may turn to unstable chaotic ones and vice verse. But most importantly, new types of motion emanate via bifurcations (or branching) of periodic orbits. The bifurcation theory of Hamiltonian dynamical systems has mainly been developed in the last half of the twentieth century.[68] One important outcome of the theory is the identification of the elementary bifurcations, which are described by very simple Hamiltonians. In spite of their simplicity, they can also be found in complex dynamical systems at critical energies. This makes elementary bifurcations generic. For molecular Hamiltonian systems, we have identified the center-saddle,[76] period doubling, pitchfork, and Hopf-like elementary bifurcations.

Bifurcation (branching) phenomena, i.e. the appearance of new motions and the change of geometry of the old orbits by varying the energy or parameters of the system, are well-known in vibrational spectroscopy. For example, the transition from normal to local mode oscillations, first discovered in symmetric ABA molecules, can be understood in classical mechanical phase space as an elementary pitchfork bifurcation.[77,78] The original local mode models included just the stretching vibrations,[79] but they were extended to include bending vibrations as well.[80,81] In what follows, we show that the notion of a local mode is more general and it is associated with the bifurcations of classical mechanical stationary objects, such as periodic orbits and reduced dimension tori.[82,83] Elementary bifurcations are very common in excited polyatomic molecules, with the simplest one, the center-saddle, being ubiquitous. By studying periodic orbits in a parameter space, we discover their bifurcations and possible localized eigenstates along them. Periodic orbits which emerge from center-saddle bifurcations appear abruptly at some critical values of the energy, usually in pairs, and change drastically the phase space around them. They penetrate in regions of nuclear phase space which the normal mode motions cannot reach. Center-saddle bifurcations are of generic type; that is, they are robust and remain for small (perturbative) changes of the potential function.[84,85] To the best of our knowledge, HCP was the first molecule where CS bifurcations were identified spectroscopically (ref 9 and references therein). Further studies of HOCl, HOBr, and HCN showed that cascades of CS bifurcations pave the road to dissociation or isomerization, as the molecule is excited along the reaction coordinate. This work has been reviewed in previous publications.[10,11]

The purpose of the present article is to review recent theoretical and spectroscopic studies, emphasizing the importance of nonlinear mechanics for assigning the spectra and extracting the dynamics of polyatomic molecules. Particularly, we demonstrate the importance of bifurcations in spectroscopy. The article is organized as follows. The three next sections introduce the theoretical approaches, which include quantum, semiclassical, and classical nonlinear mechanics. Specifically, section 2 describes *global* and spectroscopic Hamiltonians and section 3 quantum and

semiclassical calculations for the vibrational eigenstates. In section 4 we introduce the concepts of elementary bifurcations and we present our strategy to locate periodic orbits in multidimensional Hamiltonians and for general coordinate systems. In sections 5 and 6, results from triatomic and polyatomic molecules are presented, respectively. We conclude with section 7.

2. Global and Spectroscopic Hamiltonians

A prerequisite for studying the dynamics of a molecule in a specific electronic state is a reliable PES.[86,87] For the study of highly excited vibrational states, accurate potential functions over an extended nuclear configuration space are essential. Therefore, *global* PESs which describe correctly dissociation channels, isomers of the molecule, and isomerization pathways are needed. The choice of the nuclear coordinate system is crucial for expressing the potential energy surface and the nuclear Hamiltonian. Valence coordinates, i.e. bond lengths and angles, which portray the stable chemical structures, and Jacobi coordinates are among the most popular, although several others have been proposed[88] depending on the kind of dynamics we want to study (isomerization, photodissociation, scattering). For triatomic molecules, Jacobi coordinates are defined with the vectors along the diatom AB ($\vec{r}$) and the center of mass of AB to atom C ($\vec{R}$). γ is the angle between these two vectors. This coordinate system is preferred for describing the dissociation channel of atom C from the diatom AB, and the Hamiltonian operator takes a rather simple form for zero total angular momentum

$$\hat{H} = -\frac{\hbar^2}{2\mu_{C-AB}}\frac{\partial^2}{\partial R^2} - \frac{\hbar^2}{2\mu_{AB}}\frac{\partial^2}{\partial r^2} + {}^1/_2\left(\frac{1}{\mu_{C-AB}R^2} + \frac{1}{\mu_{AB}r^2}\right)\hat{j}^2 + V(R,r,\gamma) \quad (1)$$

μ_{C-AB} and μ_{AB} are the reduced masses of atom C with the diatom AB and AB, respectively. $\hat{j}$ denotes the diatomic rotational angular momentum operator, and $V(R,r,\gamma)$ the PES. Jacobi vectors can be defined for larger polyatomic molecules, thus providing a systematic way to describe the nuclear configuration space.

With the current computational power, *ab initio* electronic structure calculations are the means for producing *global* PESs for triatomic molecules with light atoms by computing thousands of energies. Reliable and efficient quantum chemistry electronic structure packages exist which allow us to carry out calculations at several levels of approximation. Among the many available for research, in our groups we use MOLPRO,[89] TURBOMOLE,[90,91] and GAUSSIAN.[92]

After obtaining the electronic energies over a predefined grid of nuclear configuration points, the practice is to fit them to an analytical function of the nuclear coordinates.[86] In a classical mechanical approximation of molecular dynamics, we need the energies and the first derivatives (forces) to integrate the equations of motion and, as we shall see, the second derivatives in optimization problems. In quantum dynamics, only the energies are needed. We must mention that, with the evolution of computers, calculations *on the fly*, i.e. to compute the forces directly with the quantum chemistry electronic structure programs as the trajectory evolves in time, become feasible.[93]

However, most frequently interpolation functions are constructed with many body expansion[86,94] and cubic spline methods. Assuming that the PES of a triatomic molecule is expressed in the R_i, $i = 1 - 3$, coordinates, the many body expansion implies

$$V = \frac{1}{2!}\sum_{i,j}\left(\frac{\partial^2 U}{\partial R_i \partial R_j}\right)_0 \Delta R_i \Delta R_j + \frac{1}{3!}\sum_{i,j,k}\left(\frac{\partial^3 U}{\partial R_i \partial R_j \partial R_k}\right)_0 \Delta R_i \Delta R_j \Delta R_k + \ldots \quad (2)$$

where $\Delta R_i = R_i - R_i^0$ with R_i^0 being the values of the coordinates at an equilibrium point of the PES. Examples of this method are the PES of HCP,[95] SO_2,[78] HCO,[35,96] and several states of ozone,[97,98] whereas the cubic spline interpolation method was used for the ground state of ozone.[99]

For large polyatomic molecules, such as biomolecules, a *global ab initio* PES is out of current computational capabilities, and thus, analytical functions are used with several parameters to fit local experimental and theoretical data such as minima and barriers. Functions based on force fields[100−102] are the most common.[103,104]

In spite of the progress in *ab initio* electronic structure calculations and the predictive power of the *global* PES, the computational burden for obtaining experimental accuracy in spectroscopy and chemical dynamics is huge, even for triatomic molecules. Thus, local spectroscopic (effective) Hamiltonians extracted with perturbative[63] or algebraic methods[105] are fitted to *ab initio* or experimental spectra. The spectroscopic Hamiltonians are usually written as the sum of a diagonal term, H_D, and a nondiagonal resonance term, H_R,

$$H = H_D + H_R \quad (3)$$

H_D denotes the Dunham expansion

$$H_D = \sum_i \omega_i I_i + \sum_{i,k} x_{ik} I_i I_k + \sum_{i,k,m} y_{ikm} I_i I_k I_m + \ldots \quad (4)$$

In our notation, H_D and the terms on the right may be considered to represent operators or the diagonal matrix elements, $\langle n_i|\hat{H}_D|n_i\rangle$, in a basis set expansion of the i^{th} harmonic oscillator's eigenfunctions. The constants (x_{ik},y_{ikm}) are fitted to spectroscopic data and

$$I_i = \frac{1}{2}(p_i^2 + q_i^2) = a_i^\dagger a_i + \frac{d_i}{2} = n_i + \frac{d_i}{2} \quad (5)$$

The I_i are defined with respect to the set of conjugate dimensionless normal coordinates for mode i, (p_i,q_i), or the creation and annihilation operators,

$$a_i^\dagger|n_i\rangle = \sqrt{n_i + 1}\,|n_i + 1\rangle;\ a_i|n_i\rangle = \sqrt{n_i}\,|n_i - 1\rangle \quad (6)$$

where n_i is the number of quanta in the i^{th} oscillator. d_i denotes the degeneracy of quantum levels (for example, in linear molecules d_i is 1 for the stretching modes but 2 for the bending modes).

The nondiagonal matrix elements of the Hamiltonian are a sum of nonlinear resonances $V_R(a_i,a_i^\dagger)$, i.e.,

$$H_R = \sum_R c_R V_R(a_i, a_i^\dagger) \quad (7)$$

A resonance among N vibrational modes implies the relation

$$m_1\omega_1 + m_2\omega_2 + ... + m_N\omega_N = m\bullet\omega \approx 0 \quad (8)$$

where m_i are integer numbers and ω_i are the frequencies of the N vibrational modes. Symbols without indexes denote vectors and • denotes the inner product between two vectors. An example is a (1:2) Fermi resonance between a stretch and a bend oscillation ($\omega_s - 2\omega_b \approx 0$) with the coupling term written as

$$V_F = c_F(a_b a_b a_s^\dagger + a_b^\dagger a_b^\dagger a_s) \quad (9)$$

Similarly, for a Darling−Dennison coupling between a symmetric and an antisymmetric stretch ($2\omega_s - 2\omega_a \approx 0$), the resonance term is

$$V_{DD} = c_{DD}(a_s^\dagger a_s^\dagger a_a a_a + a_s a_s a_a^\dagger a_a^\dagger) \quad (10)$$

Diagonalizing the quantum mechanical Hamiltonian matrix, eigenenergies and eigenfunctions are obtained in the basis set chosen (i.e., harmonic). It is straightforward to transform the quantum mechanical Hamiltonian to its semiclassical analogue by employing the Heisenberg correspondence principle, according to which the creation and annihilation operators are related to the action and angle variables (I_i,ϕ_i) by

$$a_i^\dagger \rightarrow \sqrt{I_i}\exp(-i\phi),\ a_i \rightarrow \sqrt{I_i}\exp(i\phi) \quad (11)$$

Here the i in the exponentials means $i = (-1)^{1/2}$. I_i is now the classical action integral for mode i and the relation $I_i = n_i + d_i/2$ is the Einstein−Brillouin−Keller (EBK) quantization rule for this mode.[19,18,106] Using the above definitions, we can prove that the semiclassical approximation of the resonance term in the Hamiltonian takes the form

$$H_R(I,\phi) = 2\sum_R c_R(\prod_i I_i^{|m_i|/2})\cos(m\bullet\phi) \quad (12)$$

For example, the semiclassical Fermi resonance is written as

$$V_F = 2c_F I_b\sqrt{I_s}\cos(\phi_s - 2\phi_b) \quad (13)$$

By construction the spectroscopic Hamiltonian has conserved good quantum numbers that assist us to reduce the dimensionality of the problem. The polyad quantum number, which is the total number of quanta in the excited molecule, is an example. A vector model for obtaining the constants of motion in a systematic way has been developed by Kellman[107] and by Fried and Ezra[108] and has been extensively applied by others.[59−61]

3. Quantum and Semiclassical Vibrational Eigenstates

Solving the Schrödinger equation with a *global* PES is a challenging problem that involves three steps: (i) the expression of the kinetic operator in the chosen nuclear coordinate system, (ii) the expansion of the wave function in a basis set or discretizing the wave function in a coordinate grid, and (iii) diagonalization of the Hamiltonian matrix or the time propagation of an initial wave packet. It turns out that the methods that have prevailed are those based on discretizing the wave function using uniform grids or the roots of orthonormal polynomials such as Legendre polynomials for the bend angles.

The discrete variable representation (DVR) method is the most popular one for solving the vibrational Schrödinger equation in triatomic molecules.[109] Finite difference (FD) methods stand as an appealing alternative technique for the Schrödinger equation by means of a discretization procedure. The method is introduced as a *local* approximation of the wave function $\Psi(x)$, which is interpolated at the grid points (N) with an ensemble of N Lagrange polynomial functions of order N_s. This means that only information from the neighboring points is needed. The accuracy of the approximation converges very fast with the number of terms N_s.[110] Choosing properly the grid points, the FD method would be equivalent to a pseudospectral method (PS) in the limit $N_s \rightarrow N$, but of course, the computational cost would be increased, and calculations may take considerable memory and time. Besides, although the convergence is not so fast as in PS, FD methods allow a flexible selection of discretization points.[111−113] FD approximations have led to efficient parallelized computer codes.[54,114−118]

Our ability to calculate hundreds of vibrational levels was enhanced further by introducing iterative methods in solving the diagonalization problem, such as Lanczos and the filter diagonalization method.[119−126] The traditional approach for diagonalizing the Hamiltonian matrix is based on the Householder method,[127] which yields the complete list of eigenvalues and eigenfunctions. However, this robust and accurate method becomes inadequate when the dimension of the matrix increases beyond 10000, because of unfavorable scaling laws in both arithmetic operations and memory. In the filter diagonalization method, optimally adapted basis functions, the so-called *window basis functions* Ψ_i, which span only a relatively small subspace of the whole Hilbert space, are first generated by applying the Green's function

$$\hat{G}^+(E_i) = (E_i - \hat{H} + iW)^{-1} \quad (14)$$

as a filtering operator onto an initial wavepacket χ,

$$\Psi_i = Im\hat{G}^+\chi \quad (15)$$

where iW is a complex absorbing potential ($W = 0$ for bound-states calculations). The energies E_i are taken to be equally spaced in the interval [E_{min},E_{max}]. The filtering is efficiently performed using the modified Chebychev polynomial expansion of the Green's function. In the second step, the eigenstates in the energy window [E_{min},E_{max}] are calculated by diagonalizing the Hamiltonian in the small set of basis functions, Ψ_i.

Another method employed for diagonalizing the Hamiltonian matrix is the Lanczos algorithm.[128,129] This recursive method is based on Krylov subspaces,[130] such as suggested by Lanczos.[128] The basic idea is to recursively generate a small number of vectors that span the eigenspace of interest, rendering a relatively easy diagonalization of a smaller and/or more-sparse matrix. Because of the recursive nature, these methods typically have more favorable scaling laws. The diagonalization of the tridiagonal Lanczos matrix, which is relatively straightforward, yields approximate eigenvalues.

In some cases, the eigenfunctions are needed. They can be obtained using an additional Lanczos recursion with the eigenvectors determined in the first recursion. An interesting observation is that the eigenvalues near the spectral extrema converge relatively quickly. As a result, the Lanczos method is particularly efficient for low-lying eigenvalues. The Lanczos method requires only two vectors to be stored in the fast memory, because only the action of the Hamiltonian must be computed. The latter operation relies on matrix-vector multiplication, which is particularly advantageous if the matrix is sparse or factorizable. For these reasons, the Lanczos method is ideally suited for large dimensional problems such as those met in polyatomic molecules. In addition, it is possible to calculate transition amplitudes directly using the Lanczos method without explicit calculation of the eigenstates.[131,132]

Application of semiclassical theories to effective spectroscopic Hamiltonians is a well-established tool for the investigation of vibrational systems with two or three degrees of freedom. For example, in triatomic molecules, in many cases, the high frequency mode is considered decoupled, whereas the other two provide the fast and slow modes. The conservation of the polyad quantum number assists us to reduce the semiclassical quantization just in one degree of freedom, as we can conclude from the following equations.

If u denotes the uncoupled degree of freedom and f and s denote the fast and slow degrees of freedom, respectively, then we define the action-angle variables (I_s,ϕ_s), (I_f,ϕ_f), and (I_u,ϕ_u). For a Fermi resonance (eq 9), the conserved polyad quantum number is

$$P = 2n_f + n_s \tag{16}$$

where n_s and n_f are the number of quanta in the slow and fast degrees of freedom. Introducing the canonical transformation[62]

$$(J_u, \psi_u) = (I_u, \phi_u) \tag{17}$$

$$(J_P, \psi_P) = (2I_f + I_s, \phi_s) \tag{18}$$

$$(J_0, \psi_0) = (2I_f, \phi_s - \phi_f/2) \tag{19}$$

we produce a new Hamiltonian which is only a function of the angle ψ_0

$$H_F = K_0(J_P - J_0)\sqrt{J_0}\cos(2\psi_0) \tag{20}$$

whereas the transformed diagonal term in the effective Hamiltonian (H_D) remains a function of the action variables (J_u,J_P,J_0). These actions are quantized according to the EBK condition

$$J_u = n_u + \frac{d_u}{2} \tag{21}$$

$$J_P = P + d_f + \frac{d_s}{2} \tag{22}$$

$$\mathcal{J} = \mathcal{J}(E, J_u, J_P) \tag{23}$$

$$= \frac{1}{2\pi}\int_0^{\pi} J_0\, d\psi_0 = n + \frac{1}{2} \tag{24}$$

Thus, for given quantum numbers of the uncoupled degree of freedom, n_u, and polyad P, the quantum levels are semiclassically assigned with the quantized values of the action. The corresponding eigenfunctions can be extracted approximately by transforming back to the mass weighted Cartesian coordinates of the harmonic oscillators. The method has been applied to HOBr,[133] where it can be seen that the semiclassical wave functions are symmetric, thus revealing the approximate character of the method and the nonlinear relationship between normal and internal coordinates.

Jung and Taylor[60] have introduced a promising method for assigning the quantum states in a polyad by establishing the correspondence

$$|n\rangle \rightarrow \chi_n(\phi) = \exp(in\phi) \tag{25}$$

between quantum basis set functions $|n\rangle$ (i.e., the eigenstates of the zero order Hamiltonian H_D in eq 3) and the functions χ of the angle variables. In other words, the eigenfunctions of the full Hamiltonian, $|\Psi_k\rangle$, correspond to the semiclassical functions $\Psi_k(\phi)$, i.e.,

$$|\Psi_k\rangle = \sum_n c_{k,n}|n\rangle \rightarrow \sum_n c_{k,n}\chi_n(\phi) = \Psi_k(\phi) \tag{26}$$

In fact, the transition to the semiclassical eigenfunctions is done in the reduced dimension space after a canonical transformation of the Hamiltonian in a form that takes into account the conservation of the polyad quantum numbers.

The assignment of the eigenfunctions in a given polyad is obtained by plotting the density and the phase of the semiclassical functions with respect to the angle variables ϕ and counting the nodes along the angles. We expect some regularity of the semiclassical functions because of their localization in the resonance region of phase space. To visualize the motions of the atoms in real space, a transformation back to normal coordinates, assuming the harmonic approximation, may be carried out as before. This process is called *lift*. The method has successfully been applied to DCO,[60,134] CHBrClF,[60,134] $SCCl_2$,[135] and the bending spectrum of acetylene.[60]

Apparently, since the method is based on the visual examination of the wave functions, the reduced dimension problem is restricted at most to three. Moreover, the recognition of the classical stationary objects, named by the investigators *organizing structures*, that cause localization should be identified for an unambiguous assignment. In other words, understanding nonlinear mechanics is essential, despite the authors' arguments that their method does not require knowledge of nonlinear mechanics.[60]

Recently, new approaches have been proposed for assigning the states and extracting the dynamics of vibrationally highly excited polyatomic molecules,[61] that promise to be free of the limitations of the procedure of Jung and Taylor. One of the first criteria introduced by Keshavamurthy and co-workers was based on studying the eigenstate expectation value of the resonance operator.[136−139] Applications to molecules such as DCO, CHBrClF, and C_2H_2 with reduced dimensional Hamiltonians of two degrees of freedom have shown that it is possible to dynamically assign the quantum states. This work has also demonstrated that the expectation values can detect bifurcations and identify the birth of new modes.

In a very recent paper Manikandan et al.[61] introduced a method based on time-frequency analysis[70,140−143] to plot the resonance (Arnold) web up to a maximum order, and then

Table 1. Examples of Potential Functions Which Show Elementary Bifurcations of Equilibrium Points and Periodic Orbits

bifurcation	potential
center-saddle[147]	$V(q) = \frac{1}{3}q^3 - \frac{1}{2}\alpha q^2 - \beta q - \gamma$
pitchfork[147]	$V(q) = \frac{1}{4}q^4 - \frac{1}{3}\alpha q^3 - \frac{1}{2}\beta q^2 - \gamma q - \delta$
period doubling and m:n resonances[148]	$V(x,y) = \frac{1}{2}(\omega_x^2 x^2 + \omega_y^2 y^2) + \varepsilon x^2 y$
complex unstable[149] (Hamiltonian Hopf)	$V(x,y,z) = \frac{1}{2}(\omega_x^2 x^2 + \omega_y^2 y^2 + \omega_z^2 z^2) - \varepsilon x^2 y - \eta x^2 z$

they *lift* the quantum eigenstates onto this resonance web, thus identifying the resonances that influence the eigenstate. Martens et al.[70] were the first who employed local frequency analysis to study the phase space structure for a three-mode model of the OCS molecule. Several methods[140,144,145] have been proposed to obtain the time-dependent frequencies, and Manikandan et al.[61] follow the approach based on a wavelet analysis.[145] Keshavamurthy and co-workers construct the dynamical web by the following procedure. Several trajectories at constant total energy and polyad numbers are propagated and followed in the space of appropriately chosen, independent frequency ratios. Depending on the number of degrees of freedom, one can have several such spaces. For each trajectory, the total number of visits to a given region of the frequency ratio space is recorded. The density plot, created by averaging and normalizing the number of visits over all the trajectories, yields the resonance web. It is shown that the lifting of quantum eigenstates into the resonance web reveals the classical resonances that influence the eigenstates. Results for the CDBrClF and CF_3CHFI molecules obtained by employing spectroscopic Hamiltonians and reduced 3D space are presented in ref 61.

It is known that periodic orbits exist at the center of nonlinear resonances. Therefore, constructing a plot based on periodic orbits that exist in a range of energies, we sketch the resonance web of Keshavamurthy and co-workers. As a matter of fact, the above-mentioned approaches for extracting the dynamics from the quantum eigenstates rely on the existence of stationary classical objects which act as organizing centers in phase space. For more than a century mathematicians have explored dynamical systems, and now we have theories for a systematic search of the phase space structure. In the following section we present in brief the bifurcation theory of Hamiltonian systems.

4. Elementary Bifurcations of Equilibria and Periodic Orbits

Generally, we do not expect significant changes in the topography of a molecular potential energy surface as its parameters are varied. Minima, saddles, and maxima will smoothly change their energies and positions, but they will remain minima, saddles, and maxima. However, it does happen at some critical values of the parameters to observe catastrophic changes such as the conversion of a minimum to a saddle and then to a maximum with the simultaneous appearance of two new minima. This kind of branching we call bifurcation. Similar behaviors can be traced in classical trajectories such as periodic orbits and tori. Regular trajectories which stay close to the above stationary objects may turn chaotic and escape after the event of a bifurcation. Obviously, bifurcation phenomena lead to significant qualitative changes in the dynamics. They are of great importance in celestial mechanics, and it turns out that they are important for molecules, too, provided quantum mechanics show a correspondence.

We call those bifurcations elementary which appear in the simplest nonlinear systems by varying one or two parameters. Comparing these systems with the complicated multidimensional molecular PES, we may think that a simple one-dimensional Hamiltonian is only of pedagogical use. This is not true, since we can show that, at the critical value of the parameter at which a bifurcation occurs, even a multidimensional system can be reduced to one of lower dimension by using the central manifold theorem, and then we can transform it by using normal forms into a simple Hamiltonian.[7] The mathematical theory of bifurcations in dynamical systems is well developed, and there are excellent books[6,7] and review articles[146] to introduce the subject. In this section we discuss how bifurcations appear in the simplest nonlinear Hamiltonians, those with a cubic or quartic potential. Afterward, we demonstrate that the same bifurcations do occur in the periodic orbits of molecules with three and more degrees of freedom.

In Table 1 we summarize the elementary bifurcations and example potentials which develop these bifurcations. Explanations will be given in the following sections.

4.1. Model Hamiltonians

For a system of one degree of freedom with a Hamiltonian

$$H(q,p) = \frac{1}{2}p^2 + V(q) \tag{27}$$

the trajectories are calculated by integrating Hamilton's equations

$$\dot{q} = \frac{dH}{dp} \tag{28}$$

$$\dot{p} = -\frac{dH}{dq} \tag{29}$$

q is the generalized coordinate and p its conjugate momentum. The stationary (equilibrium) points are located by requiring $\dot{q} = \dot{p} = 0$, which implies $p = 0$ and $dV(q)/dq = 0$; that is, the roots of the force (generally a nonlinear equation) are the equilibrium points of the system.[150,151]

By taking a general cubic potential,

$$V(q) = \frac{1}{3}q^3 - \frac{1}{2}\alpha q^2 - \beta q - \gamma \tag{30}$$

the equilibrium points are then the roots of the quadratic equation

$$dV(q)/dq = q^2 - \alpha q - \beta = 0 \tag{31}$$

with a discriminant defined as

$$D = \alpha^2 + 4\beta \tag{32}$$

In order that eq 31 has two real roots (equilibrium points), $D \geq 0$ is required. Thus, the parabola $D = 0$ defines the region in the two-parameter space, (β,α), where these two roots exist. Assuming $\alpha = 0$, Figure 2 shows the evolution of the two equilibria by varying the parameter β. This graph is a typical *continuation/bifurcation diagram* (CB) that depicts a center-saddle bifurcation. We notice that there are no equilibrium points for negative values of β and that at $\beta = 0$ the double root signals the genesis of the center-saddle bifurcation. The two branches correspond to stable (solid line) and to unstable (dashed line) equilibrium points. Stable means that trajectories close to this point will remain in the nearby region, whereas unstable points mean that nearby trajectories will deviate from them.

By plotting the potential function for several values of β, we can identify the minima and saddles. For $\beta < 0$, there are no equilibrium points; for $\beta > 0$, there are two equilibrium points, one minimum and one maximum; and for $\beta = 0$, there is only a saddle at $q = 0$. For nonzero values of α, the CB diagram remains the same, since by translating the origin of the coordinate to zero ($q' = q - \alpha/2$; $\beta' = \beta + \alpha^2/4$), we take the standard form of the center-saddle bifurcation, $q'^2 - \beta' = 0$. In Figure 3 several trajectories are plotted for $\beta = 1$ in the phase plane, (q,p). The dashed line denotes the separatrix of the two types of motions allowed for this dynamical system: closed stable orbits and unbound orbits. This phase space graph is typical of a center-saddle bifurcation.

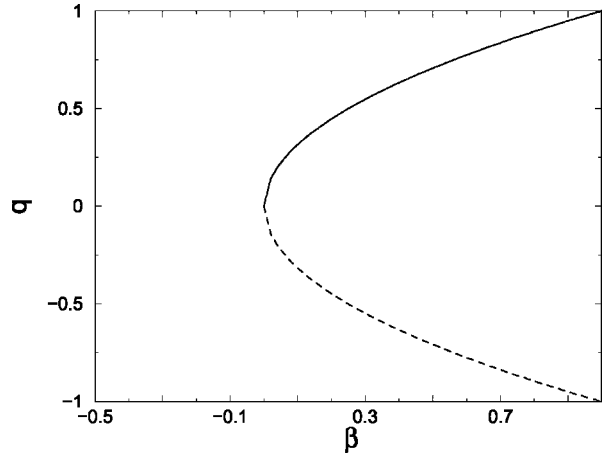

Figure 2. Continuation/bifurcation diagram for a center-saddle bifurcation of a cubic potential (Table 1). The coordinates q of the two equilibria are shown as a function of the parameter β and for $\alpha = 0$. The continuous line denotes the stable equilibrium point (minimum) and the dashed line the unstable equilibrium point (maximum). Reprinted with permission from ref 147. Copyright 2006 World Scientific Publishing Company.

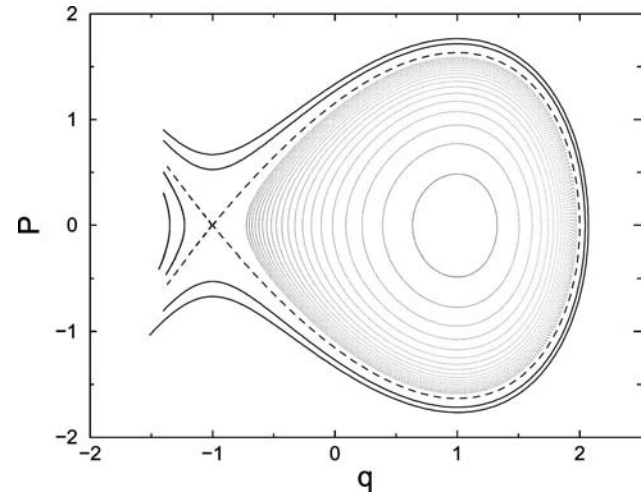

Figure 3. Trajectories which portray the phase space structure in the region of a center-saddle (CS) bifurcation ($\beta = 1$). Reprinted with permission from ref 147. Copyright 2006 World Scientific Publishing Company.

For the case of a quartic potential

$$V(q) = \frac{1}{4}q^4 - \frac{1}{3}\alpha q^3 - \frac{1}{2}\beta q^2 - \gamma q - \delta \tag{33}$$

the equilibrium points are given by

$$dV(q)/dq = q^3 - \alpha q^2 - \beta q - \gamma = 0 \tag{34}$$

This cubic equation can be reduced to a two-parameter equation by the transformations

$$x = q - \alpha/3 \tag{35}$$

$$\mu = \frac{\alpha^3}{3} + \beta \tag{36}$$

$$\lambda = \frac{2\alpha^3}{27} + \frac{\alpha\beta}{3} + \gamma \tag{37}$$

The reduced cubic polynomial is

$$x^3 - \mu x - \lambda = 0 \tag{38}$$

and the discriminant is defined by

$$D = -\frac{\mu^3}{27} + \frac{\lambda}{4} \tag{39}$$

The roots of eq 38 are as follows:
(i) one real root and two imaginary for $D > 0$,
(ii) three different real roots for $D < 0$, and
(iii) three real roots, with two of them being equal for $D = 0$. Plotting the discriminant in the parameter space (λ,μ), we get a cusp curve that defines the values of (λ,μ) where the discriminant is zero. Thus, crossing this curve from positive to negative values of D, we pass from one to three

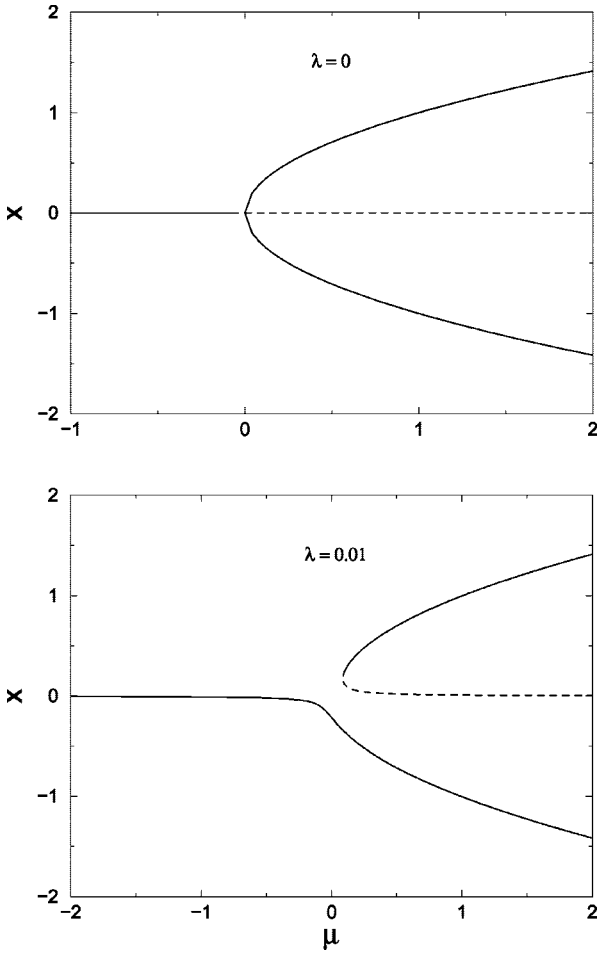

Figure 4. Continuation/bifurcation diagrams of a quartic potential (Table 1) by varying the parameter μ. $\lambda = 0$ portrays a pitchfork bifurcation and $\lambda = 0.01$ a CS bifurcation. Continuous lines denote stable equilibria and dashed lines the unstable equilibrium points. Reprinted with permission from ref 147. Copyright 2006 World Scientific Publishing Company.

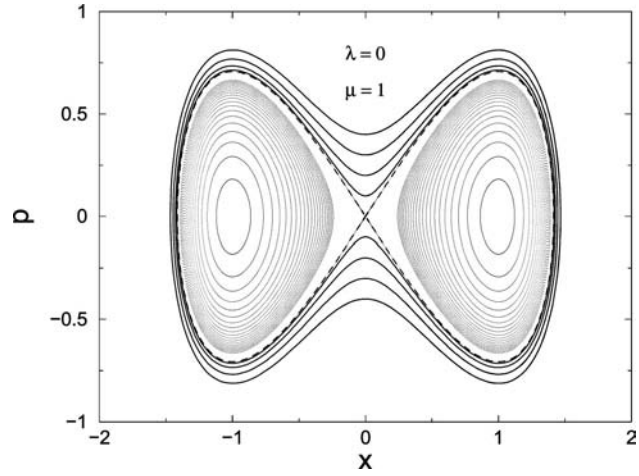

Figure 5. Phase space structure of a pitchfork bifurcation that corresponds to a symmetric double well quartic potential. Reprinted with permission from ref 147. Copyright 2006 World Scientific Publishing Company.

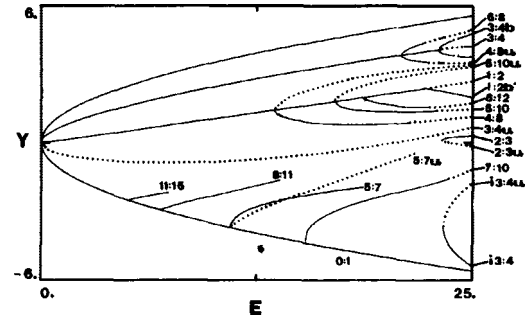

Figure 6. Continuation/bifurcation diagram in the (E,y) plane for the 2D potential given in Table 1. The labels (m:n) denote the resonance condition between the two vibrational modes in the principal families and the most important bifurcations (branches). Solid lines correspond to stable periodic orbits, dashed lines to unstable. Each point on the curve corresponds to a periodic orbit with initial conditions $x = 0$ and p_x determined from the conservation of total energy. Reprinted with permission from ref 148. Copyright 1989 American Institute of Physics.

equilibrium points. A double degeneracy of equilibrium points is encountered on the cusp curve.

The CB diagram for $\lambda = 0$ and varying the parameter μ is shown in Figure 4. This is a typical pitchfork bifurcation. The introduction of a second parameter ($\lambda \neq 0$) alters the CB diagram as shown in Figure 4. Comparing the two continuation/bifurcation diagrams for $\lambda = 0$ and $\lambda \neq 0$, we can see that the unstable branch in the pitchfork bifurcation (dashed line) becomes the unstable branch of a CS bifurcation, whereas one stable branch in the pitchfork bifurcation is the stable branch of the CS bifurcation. We can also see that the parent family in the pitchfork bifurcation evolves to a *hysteresis*. We can think of this continuation/bifurcation diagram as a folded surface in the (λ,μ,x) space. The size of the gap in the CB curves depends on the value of the parameter λ.

The three equilibria in the quartic potential are two minima and one maximum. Trajectories plotted in the phase plane (x,p) are shown in Figure 5 for the symmetric double well potential ($\lambda = 0$ and $\mu = 1$). The separatrix (dashed line) emanates from the maximum of the potential, and it separates the two types of motion encountered in this system.

4.2. Periodic Orbits

Systems of one degree of freedom are integrable, and bound trajectories are periodic. Moving to two degrees of freedom and correspondingly to a four dimensional phase space, a totally new world is opened with periodic orbits, tori, chaotic trajectories, homoclinic and heteroclinic orbits, and cantori. Several books describe all these classical mechanical objects at different levels of mathematical rigor and comprehension.[6,7,152]

The 2D model potential with the cubic coupling term given in Table 1 is one of the most studied by both the astrophysical and molecular communities. Values for the parameters (ω_1, ω_2, ε) in the potential are given in ref 148. From the bifurcation diagram shown in Figure 6 (Figure 1 in ref 148), new periodic orbits emerge every time the frequencies become commensurate ($m\omega_1 + n\omega_2 = 0$) as energy varies. These families of periodic orbits are predicted from the theorems of Poincaré-Birkoff,[153] which state that commensurate tori are destroyed to produce stable and unstable POs.

The theory of periodic orbits was mainly developed to study celestial mechanics. However, we can see the relevance

of periodic orbits to molecules by inspecting the semiclassical formula of the quantum propagator, the Fourier transform of which provides the density of states[19,154]

$$\langle q_2|\exp(-i\hat{H}t/\hbar)|q_1\rangle = \sum_{\text{roots}}\left[(2\pi i\hbar)^N\left|\frac{\partial q_2}{\partial p_1}\right|\right]^{-1/2}\exp(iS(q_2,q_1,t)/\hbar \quad (40)$$

$\hat{H}$ is the Hamiltonian operator for a system with N degrees of freedom. q are the coordinates, and $S(q_2,q_1,t)$ is the action along the trajectories from the initial configuration point q_1 to the point q_2 arriving at the time interval t. Invoking the stationary phase approximation for trajectories returning to the initial configuration in the time period T

$$\frac{\partial S(q,q,T)}{\partial q} = 0 \quad (41)$$

and recalling some basic rules of Hamiltonian mechanics,[62] we can prove that the major contributions to the integral in eq 40 come from the periodic orbits[19]

$$\left[\frac{\partial S(q_2,q_1,T)}{\partial q_1} + \frac{\partial S(q_2,q_1,T)}{\partial q_2}\right]_{q_1=q_2=q} = p_2 - p_1 = 0 \quad (42)$$

Further support for the importance of periodic orbits in computing molecular spectra came from the scarring theory of Heller. Heller[72] demonstrated with model potentials that the eigenfunctions may stay localized around unstable periodic orbits. It turns out that the *scarring* of the wave functions by stable or the least unstable periodic orbits is a general phenomenon for polyatomic molecules, too. Overtone states are associated with isolated POs, and hence, it is important to locate those periodic orbits with the shortest periods.

For a polyatomic molecule with N degrees of freedom, q_i ($i = 1,..., N$) generalized coordinates, and p_i ($i = 1,..., N$) conjugate momenta, the location of periodic orbits requires the solution of a 2-point boundary value problem

$$x(T) - x(0) = 0 \quad (43)$$

where T is the period of time after which the trajectory obtained by integrating the equations of motion returns to its initial point in phase space, $x_0 = x(0)$. For convenience, we write coordinates and momenta as the components of the generalized coordinate vector x,

$$x = (q_1, ..., q_N, p_1, ..., p_N)^+ \quad (44)$$

where $+$ denotes the transpose of the $2N$-D column vector. The equations of motion are then written as

$$\dot{x}(t) = J\frac{\partial H(x)}{\partial x} \equiv J\partial H(x) \equiv J\nabla H(x) \quad (45)$$

where J is the symplectic matrix

$$J = \begin{pmatrix} 0_N & I_N \\ -I_N & 0_N \end{pmatrix} \quad (46)$$

0_N and I_N are the zero and unit $N \times N$ matrices, respectively.

The equilibrium points are defined by requiring $\dot{x} = 0$ or

$$\nabla H(x) = 0 \quad (47)$$

To locate a PO with a period T, we usually linearize the difference of equations of motion of two neighboring trajectories,

$$\zeta(t) = x'(t) - x(t) \quad (48)$$

for obtaining the *variational equations*

$$\dot{\zeta}(t) = J\partial^2 H(x(t))\,\zeta(t) \quad (49)$$

$\partial^2 H(x(t))$ denotes the matrix of second derivatives of the Hamiltonian evaluated at the original trajectory $x(t)$ for time t.

The general solution of eq 49 can be expressed by evaluating the fundamental matrix at time t, $Z(t)$.[155] At $t = 0$ it is valid

$$Z(0) = I_{2N} \quad (50)$$

The solution of eq 49 is then given by

$$\zeta(t) = Z(t)\,\zeta(0) \quad (51)$$

where $\zeta(0)$ describes the initial displacement from the trajectory x_0.

For periodic orbits the fundamental matrix at $t = T$,

$$M = Z(T) = \frac{\partial x(T)}{\partial x_0} \quad (52)$$

is called the *monodromy matrix*, the eigenvalues of which determine the stability of the periodic orbits.[7] Because of the symplectic property of Hamiltonian systems,[150,151] if λ_i is an eigenvalue of the monodromy matrix, then its complex conjugate λ_i^*, as well as the λ_i^{-1} and $(\lambda_i^{-1})^*$, are also eigenvalues.

The properties of the monodromy matrix and the different cases of stability have been described before.[156] For conservative Hamiltonian systems, one pair of eigenvalues of the monodromy matrix is always equal to one. For a system of three degrees of freedom, the other two pairs are represented on the complex plane, as is shown in Figure 7. As energy varies,[157] the eigenvalues of stable periodic orbits move on the unit complex circle. When the eigenvalues are out of the unit circle but on the real axis, the periodic orbit is single or double unstable, and finally four complex eigenvalues may come out of the unit circle and the PO is characterized as complex unstable. When the eigenvalues collide, new periodic orbits emerge. Collisions at $+1$ signal the birth of center-saddle or pitchfork bifurcations. Collisions at -1 give a period doubling bifurcation. Generally, every time the stability parameter of a stable PO, $\sigma = \ln(\lambda)/T$, satisfies a relation, $T/(2\pi/\sigma) = m/n$, with m and n being integers, then new periodic orbits are born with a period nT. The theory of Krein, Gelfand, and Lindskii[155] treats the change of stability of periodic orbits as the parameters of the system vary. Particularly for molecular Hamiltonians, see refs 148 and 156.

Complex instability appears in 3D Hamiltonian systems and higher and may result in the genesis of new POs or tori.[158,68] We expect this kind of bifurcation to appear more often in polyatomic molecules, but at present there is no spectroscopic manifestation of this type of bifurcation. The 3D model potential of Table 1 provides an example of a

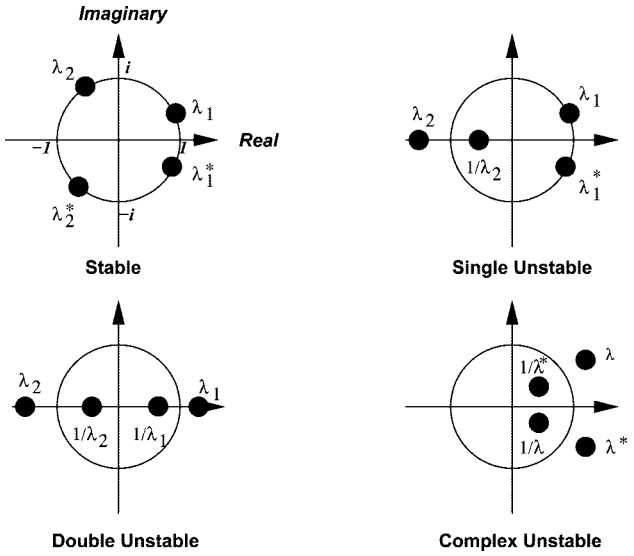

Figure 7. Eigenvalues of the monodromy matrix for a molecule with three degrees of freedom. There are three pairs of complex conjugate eigenvalues, one of which is always equal to one (not shown). The other two pairs move in the complex plane as energy varies. The positions of these eigenvalues with respect to the complex unit circle determine the stability of the PO.

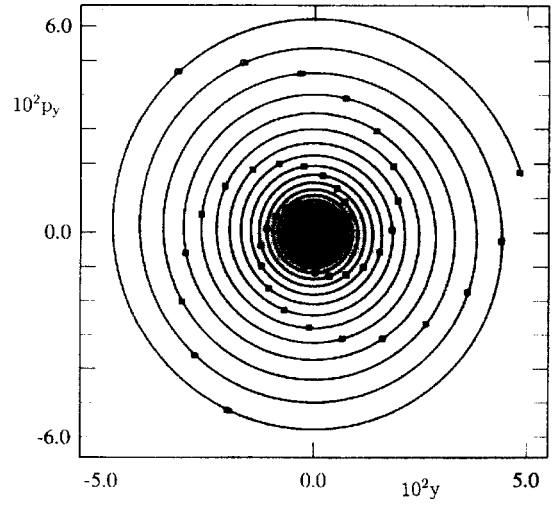

Figure 8. Projection of the spiral invariant curve from a complex unstable periodic orbit. The analytically obtained points (open squares) are compared with the numerically calculated points (filled squares), which in most cases coincide. Reprinted with permission from ref 149. Copyright 1994 The American Physical Society.

complex unstable 1:2:2 periodic orbit.[149] It was shown that nearby trajectories to this PO diverge exponentially with simultaneous rotation (Figure 8), with a frequency which is manifested by computing the quantum mechanical autocorrelation function.[149]

POMULT is a Fortran code for locating periodic orbits and equilibrium points in Hamiltonian systems based on 2-point boundary value solvers[159,160] which use multiple shooting algorithms.[161] The code has mainly been developed for locating periodic orbits in molecular Hamiltonian systems with many degrees of freedom, and it utilizes a damped Newton−Raphson method and a secant method. Stationary points and periodic orbits are located numerically with a new version of the POMULT program written in Fortran95.[162] With the multiple shooting methods, we convert the 2-point boundary value problem to *m* initial value problems; that is, we search for the appropriate initial values of coordinates and momenta that satisfy the boundary conditions and the continuity equations.[162] Analytical first and second derivatives of the potential function required for the solution of the equations of motion and the variational equations may be computed by the AUTO_DERIV program, a Fortran code for automatic differentiation of an analytic function of many variables written in Fortran.[163]

The characteristic bisection method gives an alternative algorithm for finding the roots of nonlinear algebraic and/or transcendental equations.[164] It has been applied to the LiNC/LiCN molecular system to locate periodic orbits and to construct the continuation/bifurcation diagram of the bend mode family.[165] The algorithm is based on the characteristic polyhedra, which define a domain in phase space where the topological degree is not zero. The results are compared with previous calculations obtained by the Newton multiple shooting algorithm. The characteristic bisection method not only reproduces the old results but also locates new symmetric and asymmetric families of periodic orbits of high multiplicity.[165]

5. Triatomic Molecules

Spectroscopy lightens only specific events of the molecule, leaving most of its states in the dark. Hence, spectroscopic Hamiltonians are the natural way to model molecular spectra, although they are based on assumptions such as the dimensionality of the active space and the number and nature of resonances that influence the spectrum. Global Hamiltonians, especially *ab initio*, are free of these assumptions. A global method to analyze complex spectra and understand the flow of intramolecular energy was introduced by Davis.[166] Analysis of experimental or theoretical spectra by controlling their resolution allows one to systematically unveil the parent−daughter relation of the spectral lines and progressions, which is the equivalent of following the flow of energy in time and the details of the trajectory in phase space. This method has a relation to the recently introduced methodology of Keshavamurthy and co-workers[61] which requires the construction of the resonance map via the frequency analysis of trajectories instead.

All the methods presented up to now for extracting the dynamics from complex vibrational spectra rely on revealing the classical stationary objects that localize the eigenfunctions. We believe that, as spectroscopic effective Hamiltonians cannot be produced without first identifying the equilibria of the potential energy surface, equivalently the localization of periodic orbits is a prerequisite for a profound analysis of molecular dynamics.

Over the past few years we have constructed continuation/bifurcation diagrams of periodic orbits by varying the total energy for a plethora of molecules spanning a range from conventional ones[9−11] to van der Waals clusters,[167−169] unbound molecules (FH_2),[170] and, recently, biomolecules.[103,104] All these studies demonstrate the localization of overtone states along fundamental (principal) and bifurcating POs and the universality of elementary bifurcations such as CS.

We initially determined the importance of CS bifurcations of periodic orbits in studies of the isomerization dynamics in double well potential functions.[171] These POs connect the two minima and scar the isomerizing wave functions, i.e. eigenfunctions with significant probability density in both wells. Their birth is due to the unstable periodic orbit which emanates from the saddle point of the potential energy surface. However, even below the potential barrier, a series

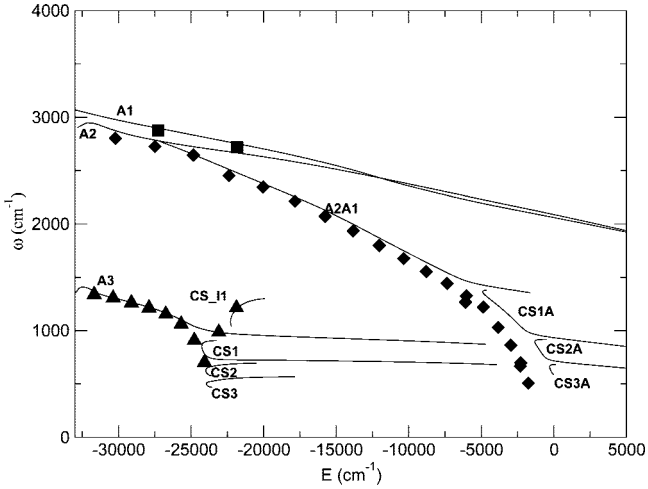

Figure 9. Periodic orbit continuation/bifurcation diagram of the $\tilde{a}^1A_1$-state of CH_2. A3 is the family that corresponds to the bend normal mode, A2 to the symmetric stretch, and A1 to the antisymmetric stretch mode. The symbols represent the energy spacings between neighboring quantum states of the overtone progressions; squares for the antisymmetric stretch, diamonds for the symmetric stretch, and triangles for the bend. CS denotes periodic orbits emanated from center-saddle bifurcations. Note that the even quantum number states for the antisymmetric stretch are shown. Reprinted with permission from ref 173. Copyright 2005 American Institute of Physics.

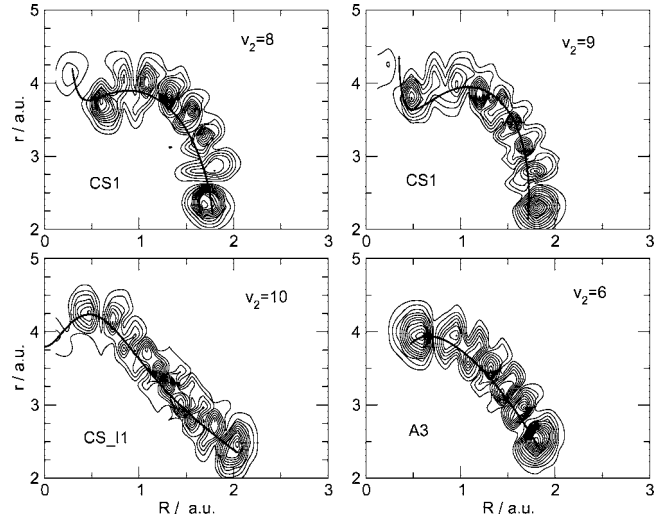

Figure 10. Regular localized wave functions of the bending mode of methylene marked by periodic orbits at approximately the same energy. Reprinted with permission from ref 172. Copyright 2004 Elsevier Publishing Company.

of CS bifurcations of periodic orbits pave the way to the isomerization process. A recent example is methylene, $CH_2(\tilde{a}^1A_1)$.[172,173]

5.1. Methylene

The 3D PES for the $\tilde{a}^1A_1$-state of CH_2 was taken from the literature.[174,175] The potential has two equivalent minima of C_{2v} symmetry separated by a linear saddle (1.095 eV). From each minimum, a number of families of stable periodic orbits emanate, at least as many as the number of normal modes, the characteristic motions of which they portray.[176] For saddle points the principal periodic orbits are unstable.[177] A projection of the continuation/bifurcation diagram of POs consists in plotting the frequencies ($\omega = 2\pi/T$) of the periodic orbits as functions of the total energy. Such a CB diagram is shown in Figure 9.[172]

The continuous lines denote the frequencies of periodic orbits as functions of the total energy E in wavenumbers. A3 is the family that corresponds to the bend normal mode, A2 to the symmetric stretch, and A1 to the antisymmetric stretch mode. The harmonic frequencies are estimated to be $\omega_1 = 3069$ cm^{-1} for the antisymmetric stretch, $\omega_2 = 2906$ cm^{-1} for the symmetric stretch, and $\omega_3 = 1382$ cm^{-1} for the bend. The continuation lines in Figure 9 do not distinguish stable from unstable POs. The A1 family remains stable for the energy range shown, but the A2 symmetric stretch family becomes early single unstable and after its bifurcation at about 0.7 eV double unstable. The bifurcating A2A1 family is initially single unstable, but it becomes stable at energies above the saddle point. The A3 is stable up to the barrier of isomerization, after which it becomes single and later double unstable. We may conclude that extended chaos sets in at energies above the barrier of linearization.

In agreement with previous studies, a cascade of CS bifurcations appears as we approach the saddle point of the linearized molecule.[9] This scenario is typical as the parent family approaches the bifurcation critical energy. Its frequency levels off and two new families appear with one branch showing high anharmonicity. As energy increases, the frequency of the daughter family with the most anharmonic behavior starts leveling off again and a new CS bifurcation takes place. The mechanism of generating this cascade of center-saddle bifurcations can be understood as a cascade of resonances between coupled oscillators.[178]

Figure 10 shows representative periodic orbits projected in the (R,r) Jacobi coordinate plane and overlaid by quantum mechanical eigenfunctions. The A1 PO has mainly excitation along the angle Jacobi coordinate. The energies of these periodic orbits are above the barrier of linearization.[179] The CS_I1 represents periodic orbits which surpass the barrier of isomerization. These POs also originate from a center-saddle bifurcation, and they mark isomerizing quantum states. Notice the low probability amplitude at the top of the barrier.

The vibrational energy levels for zero total angular momentum ($J = 0$) were determined using the recursive Lanczos algorithm.[128] A total of 602 vibrational states was found below the dissociation limit. To investigate the statistical behavior of the bound state spectrum, the nearest neighbor spacing distribution (NNSD) and the Δ_3 distribution were computed. The spectrum was first unfolded using the method of Haller et al.[180] so that the mean nearest neighbor spacing is close to unity. The NNSD is close to the Wigner distribution,[181] indicating that the short-range fluctuation of the vibrational spectrum is mostly chaotic. The long-range Δ_3 distribution[182] also indicates the dominance of the chaotic character.

The classical frequencies are compared with the energy difference between adjacent quantum eigenenergies for the three series of overtone vibrational progressions. In a rather simple approach, we compare classical and quantum mechanical eigenfrequencies by shifting the quantum energies by the zero-point-energy and we plot the energy differences with respect to the upper level. As we can see in Figure 9, the anharmonicity of the overtone states closely follows that of the frequencies of the periodic orbits. Furthermore, we conclude that, in spite of the irregular behavior predicted by the statistical measures for CH_2 ($\tilde{a}^1A_1$), the overtone states of the bending mode are regular and well localized in

configuration space up to and above the barrier to linearization (Figure 10). This was one of the conclusions of Green et al.[183] These investigators carried out an extensive *ab initio* study of the two lowest singlet excited states of methylene, $\tilde{a}^1A_1$ and $\tilde{b}^1B_1$, which are degenerate for linear geometries and are separated for planar geometries because of Renner−Teller interaction. Since this work leads to conclusions similar to ours in spite of the fact that it takes the Renner−Teller interaction into account, we may infer that there is no strong interaction between the two surfaces.

It turns out that the cascade of center-saddle bifurcations of periodic orbits is a generic mechanism to approach isomerization or dissociation thresholds, as previous studies on triatomic molecules have revealed.[9−11] The stable or the least unstable branches of these bifurcations trace the most stable regions in phase space where the quantum mechanical eigenfunctions are localized. Spectroscopic evidence for such states has been found for HCP.[9] The spectroscopic characteristic of this molecule is a 2:1 Fermi resonance between the CP stretch and bend.[59] Jacobson and Child[184,185] studied a spherical pendulum model Hamiltonian of the Fermi resonance and found the dip in the energy level spacing, which is characteristic of the saddle point. However, as the authors point out, one must be aware of the differences above the barrier states for molecules which mimic a spherical pendulum model, such as HCP, and Renner−Teller systems such as the one studied in this article. Although spectroscopic differences for these two molecules, HCP and CH_2, are expected, the classical interpretation by periodic orbits is the same; the quantum states are associated with center-saddle bifurcations. Above the barrier, the CS periodic orbits are those which connect the two minima, and they have been named isomerizing states.

An interesting question is whether CS bifurcations below and above the barrier have the same origin. Those which are born below the barrier may be thought of as the result of the rapid change in the anharmonicity along the reaction path, which brings the system into multiple resonances as energy varies. On the other hand, those above the barrier are associated with the unstable periodic orbits originated from the saddle point and the Newhouse wild hyperbolic set.[186,187] A study related to the spectral patterns of acetylene−vinylidene isomerization has been published by Yang, Tyng, and Kellman.[188]

We have also studied low-lying scattering resonances of the CH_2 system by the filter-diagonalization method based on the Chebyshev propagation, and we have examined their roles in both unimolecular and bimolecular reactions.[173] A few hundred narrow resonances were found in the energy range up to approximately 4000 cm^{-1} above the lowest dissociation asymptote. They exhibit a large variation in their widths, suggesting strong state specificity. On average, the resonance width increases with energy, but its fluctuation decreases. While the resonances are mostly isolated at lowest energies, they increasingly overlap as the energy increases. These resonances can be considered as an extension of the highly excited vibrational states above the dissociation limit and have properties that resemble those of the bound state spectrum. Indeed, analysis of the classical phase space also indicates that many periodic orbits extend smoothly into the continuum. This observation implies that a good understanding of the resonances can be achieved by studying the highly excited vibrational levels. Below 2000 cm^{-1}, where the resonances are mostly isolated, the unimolecular decay into the CH + H channels is dominated by individual CH_2 resonances. The decay of these resonances is found to conform to neither the mode-specific nor the statistical state specific limits. This is consistent with our understanding of the vibrational dynamics near the dissociation limit, which shows regularity embedded in a largely chaotic classical phase space. Indeed, the fluctuation of the resonance width is reasonably described by the Porter−Thomas distribution[189] stemming from random matrix theory. However, significant regularity persists in both highly excited bound states and low-lying resonances. In particular, we have found resonances possessing clear nodal structures related to local and hyperspherical vibrational modes. The cascade of CSiA families shown in Figure 9 converges to the dissociation limit.[173]

Because of these regular resonances, statistical theories such as the RRKM[190] and the statistical adiabatic channel model (SACM)[191] overestimate the averaged quantum decay rate in this energy range. The coexistence of regular and irregular resonance states makes the CH_2 system an intermediate case between the two limiting cases of unimolecular reactions. Like other XH_2 hydrides such as water, the CH_2 system presents an interesting case for studying mode-selective chemistry and intramolecular vibrational energy redistribution. Kinematic factors such as the mass disparity between H and X favor the existence of local modes, which in turn suggests the possibility of selectively exciting one of the two C−H bonds. For an isotopomer CHD, for example, mode-selective excitation might lead to preferential branching of the products, namely CD and CH.[2] It is interesting to note that this system differs from completely regular systems such as HCO in that the mode-selective unimolecular reaction is embedded in a largely chaotic classical phase space.

The bimolecular reaction is also dominated by resonances. The results[173] unequivocally confirm that the oscillation structure observed in bimolecular reaction probabilities is due to resonances, many of which are long-lived and overlap with each other. As a result, it is difficult to assign the peaks in the reaction probability to individual resonance states. However, the lifetimes of many resonances are sufficiently long to permit a statistical treatment of the bimolecular reaction, as illustrated in recent work by us and others.[173] Resonances affecting the bimolecular reaction exhibit very different characteristics from those that dominate the unimolecular reaction. The former are found to have significant amplitudes in both the reactant and product channels, whereas the latter deposit their energy mainly in the C−H vibration. The detailed analysis presented in this work[173] allowed us to gain deeper insight into the roles played by the long-lived resonances in both the unimolecular and bimolecular reactions.

Contrary to the CH_2 molecule, which displays strong chaotic dynamics, HCO and DCO[35,96] display regular behavior, even above the dissociation threshold, while HO_2 has regular states embedded among chaotic ones,[192] thus presenting an intermediate case. A periodic orbit analysis and a classification of the vibrational overtone levels of DCO and HCO have been presented in ref 96. For DCO the states are organized in terms of increasing polyad quantum number $P = n_1 + n_2 + n_3/2$. It was shown that the members of the pure overtone series are guided by periodic orbits, even in the continuum. Once more, it is demonstrated that the highly anharmonic states localized along the dissociation coordinate correspond to orbits originating from center-saddle bifurca-

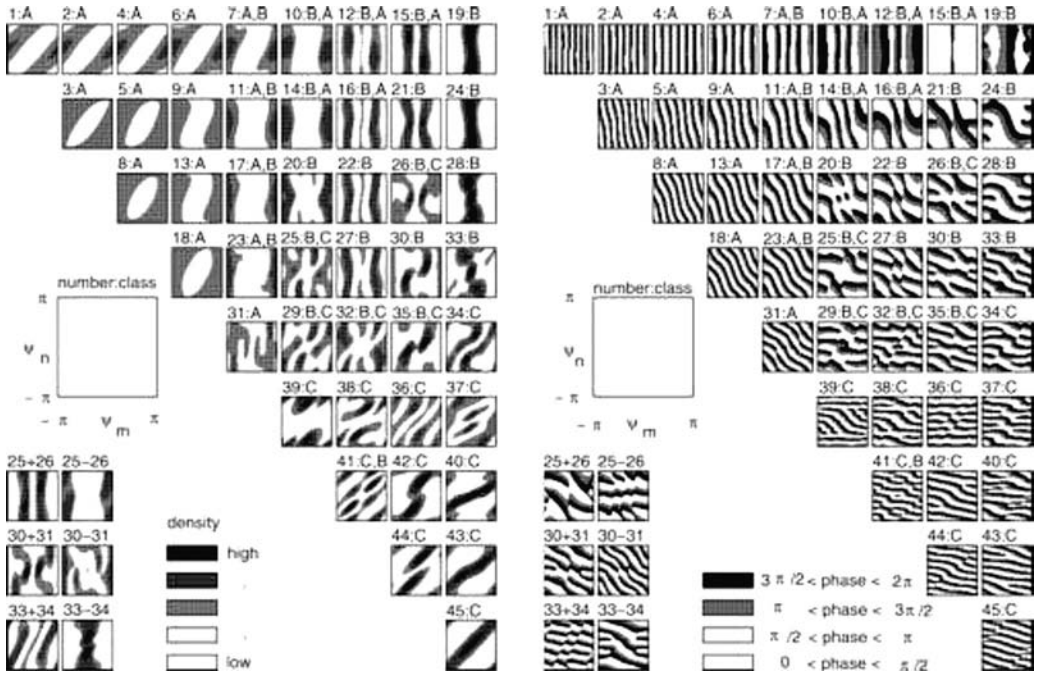

Figure 11. Part a shows the density of the semiclassical wave functions of all 45 eigenstates of polyad 8 of DCO plotted as functions of the angle variables (ψ_m,ψ_n) in the [$-\pi$,π) range. Darker gray means higher density. Each little frame is labeled above by the state and the class assigned to this state. Part b shows in exactly the same arrangement the phases of the wave functions. Here, white means phase in the interval [0,π/2), light gray means phase in the interval [π/2,π), dark gray in [π,3π/2), and black phases in [3π/2,2π). Reprinted with permission from ref 60. Copyright 2007 American Chemical Society.

tions in the classical phase space. A detailed assignment of the polyad $P = 8$ has been given by Jung, Taylor, and co-workers[60,134] using a spectroscopic Hamiltonian and their method to plot probability densities and phases of semiclassical wave functions.[60] Their results are summarized in Figure 11.

Calculations for the isotopomer molecule HCO have revealed a period doubling bifurcation of the R principal family of POs which do leave their trace on the nodal structure in a class of eigenfunctions (see Figure 5 in ref 96).

We have provided a thorough analysis of the vibrational spectrum and dynamics of the HO_2 system, based on a new and accurate potential energy surface (PES).[192] It is shown that the vibration of HO_2 is quite regular at low energies, but increased irregularity at higher energies prevents the assignment of all vibrational levels. Overall, the vibrational spectrum can be considered as an intermediate case with mixed regularity and irregularity. An interesting observation is the regularity in the OO stretch overtones up to the H + $\mathbf{O}_2$ asymptote, which is due to the emergence of center-saddle bifurcations. This conclusion is in contrast to that obtained earlier on the semiempirical double many-body expansion (DMBE) IV PES, which showed complete chaotic vibration at high energies.[193] It is not yet clear how the difference in the PES will impact the dynamics of both unimolecular reactions and bimolecular reactions. Results at $J = 0$ have demonstrated substantial changes in the reaction probability.

From the above discussion it becomes apparent that, establishing a correspondence between periodic orbits, on one hand, and quantum mechanical energy levels, on the other hand, not only provides an assignment, which is free of the coordinate system used, but also reveals details of the dynamical behavior in regions of the phase space where the dynamics is dominated by resonances. Assignments in terms of periodic orbits are often more meaningful than assignments in terms of normal mode quantum numbers. The most interesting observation is the existence of center-saddle bifurcations in the classical phase space, which lead to the birth of new state progressions at energies well above the global minimum.

5.2. Ozone

5.2.1. Ground State $O_3(X^1A_2)$

The study on the ground electronic PES of ozone was carried out with an *ab initio* potential energy surface that is *global*; that is, it covers the three identical C_{2v} (open) minima, the D_{3h} (ring) minimum, as well as the $O(^3P) + O_2(^3\Sigma_g^-)$ dissociation threshold.[99] The electronic structure calculations were performed at the multireference configuration interaction level with complete active space self-consistent field reference functions and correlation consistent polarized quadruple-ζ atomic basis functions. An analytical representation was obtained by a three-dimensional cubic spline. The calculated potential energy surface has a tiny dissociation barrier and a shallow van der Waals minimum in the exit channel. The ring minimum is separated from the three open minima by a high potential barrier and therefore presumably does not influence the low-temperature kinetics. The dissociation energy is reproduced up to 90% of the experimental value. All bound states of nonrotating ozone up to more than 99% of the dissociation energy were calculated using the filter diagonalization technique and employing Jacobi coordinates. The three lowest transition energies for $^{16}O_3$ are 1101.9 cm^{-1} (1103.14 cm^{-1}), 698.5 cm^{-1} (700.93 cm^{-1}), and 1043.9 cm^{-1} (1042.14 cm^{-1}) for the symmetric stretch, the bending, and the antisymmetric stretch modes, respectively; the numbers in parentheses are the experimental values. The root-mean-square error for all measured transition energies for $^{16}O_3$ is only 5 cm^{-1}. The comparison is equally favorable

for all other isotopomers, for which experimental frequencies are available. The assignment is made in terms of normal modes, despite the observation that with increasing energy an increasing number of states acquires local-mode character. At energies close to the threshold, a large fraction of states is still unambiguously assignable, particularly those of the overtone progressions. This is in accord with the existence of stable classical periodic orbits up to very high energies (see Figure 8 in ref 99 and also ref 194).

However, most interesting is the unusual dependence of its formation rate constants on oxygen isotopes.[195−199] For example, the ratio of the rate constants for the reactions

$$^{a}\mathrm{O} + {}^{b}\mathrm{O}^{c}\mathrm{O} + \mathrm{M} \rightarrow {}^{a}\mathrm{O}^{b}\mathrm{O}^{c}\mathrm{O} + \mathrm{M}$$

with respect to the rate constant of $^{16}O + {}^{16}O^{16}O + M$ has been found to vary between 0.92 and 1.50.[200] The slower reaction corresponds to the isotopes $^{18}O + {}^{16}O^{16}O$ and the fastest one to the isotopes $^{16}O + {}^{18}O^{18}O$. Other mass combinations give ratios between these two extreme values.

Janssen et al.[200] found a correlation with the zero point energy (ZPE) change of the oxygen molecules participating in the isotope exchange reactions. When the difference between product and reactant ZPE is positive (endothermic reaction), the lifetime of the complex increases. On the contrary, when the ZPE change is negative (exothermic), the lifetime decreases. Their argument that this correlation is related to the association reaction is based on the lifetime of the complex; the endothermicity acts as a potential barrier, and thus, the complex lives longer than in exothermic reactions.

These results inspired Schinke and co-workers[201,202] to develop a model potential that takes into account the ZPE dependence by adjusting the potential energy surface in the product channels so that the correct exothermicities and endothermicities are matched.

Marcus and co-workers[197,203,204] in a series of articles presented statistical RRKM theories[190] which satisfactorily explain a large number of experimental data. However, to accomplish the task, it was necessary to introduce ad hoc parameters to justify deviations from the statistical behavior assumed in RRKM theory. Other models have been proposed, like that of Miklavc and Pyerimhoff.[205]

In earlier studies, the explanation of the ozone isotope effect relied on the symmetry of isotopomers. However, later on, kinetic studies defied the arguments based on symmetry. The role of symmetry in the anomalous ozone mass effect reappeared in the theory of Gao and Marcus,[197] who claimed that the number of states by which the rate constants are calculated is different for the symmetric and asymmetric ozone isotopomers. Calculations on an accurate *global* potential energy surface (PES)[99,206] revealed that the dynamics of ozone to a large extent is regular, and that justifies a non-RRKM behavior.

The pertinent quantum states for the dissociation (association) of the molecules are those above the threshold energy, and resonances are responsible for long lived intermediates. Because of the localization of these resonances along periodic orbits, it would be useful to construct continuation/bifurcations diagrams for the three isotopomers of ozone, (m_3,$m_1 - m_2$) = (16,16 − 16), (16,18 − 18, and (18,16 − 16), and see how the symmetry breaking by mass substitution affects the CB diagram of the molecule. It is important for the isotopically substituted ozone to define properly the masses and coordinates. We employ Jacobi coordinates. Mass m_3 is connected with the distance (R) to the center of mass (CM) of the diatom $m_1 - m_2$ with bond length (r). The angle γ is the (m_3−CM−m_2) angle.

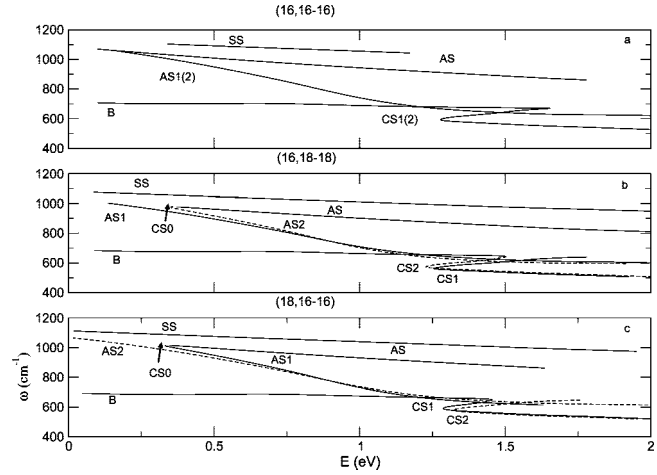

Figure 12. Continuation/bifurcation diagrams of three isotopomers of ozone in the ground electronic state (X^1A_2). SS denotes the symmetric stretch, AS the antisymmetric stretch, B the bend vibrational mode, and CS the center-saddle bifurcations.

The CB diagram for the symmetric isotopomer of ozone, (16,16 − 16), is shown in Figure 12a. SS denotes the family of POs that corresponds to the symmetric stretch normal mode, and accordingly, the AS family corresponds to the asymmetric stretch and B to the bend normal mode. At energy 0.16 eV the AS family turns from stable to unstable via a pitchfork bifurcation (AS1). The number 2 denotes that two families of periodic orbits emerge out of the bifurcation of the asymmetric stretch (AS), each of which generates later one center-saddle bifurcation, the CS1 families. The two AS1 POs have the same periods and morphologies, but they are located in different regions of phase space.

The CS1 joins the bend family (B) at an energy about 1.65 eV, giving the double center-saddle bifurcation (subcritical (evolving inward with the parameter) and supercritical (evolving outward with the parameter)). Because of the localization of the new POs, we may consider that one family of AS1 and CS1 is along the r_1 bond and the other along the bond, $r_2 = r$.

By breaking the symmetry of the molecule with the mass combination of (16,18 − 18), the pitchfork bifurcation is split to a single family which we would initially assign as the asymmetric stretch, AS1, and a center-saddle bifurcation, CS0, which appears at about 0.33 eV (Figure 12b).

For the two branches of the center-saddle bifurcation, we use the symbols AS and AS2 for the sake of a clearer correspondence with the branches in the symmetric molecule, (16,16 − 16). The AS1 is initially the stable part of the old AS and at higher energies follows one of the AS1 branches of the symmetric case. In the new born center-saddle bifurcation, CS0, the AS branch is the unstable part of the old AS and the AS2 is the second branch of the old degenerate AS1. We may think again in terms of local modes. The AS1 low frequency mode is related to the 18 − 18 oscillator and the AS2 with the 16 − 18 bond for energies below 0.9 eV. However, notice in Figure 12b that because of the frequency mismatch between AS1 and AS2 the two curves cross at about 0.9 eV. Above this energy, the AS2 POs are localized along the r bond and the AS1 along the R bond. Thus, they reverse their initial morphologies.

The breaking of degeneracy of the AS1 families in the asymmetric molecule causes lifting of degeneracy in the CS families above dissociation. We denote these center-saddle families as CS1 and CS2. The family which appears first joints smoothly the bend family, making a subcritical CS bifurcation. The CS bifurcation emerging at higher energies stays by itself at least for the energies studied. The dashed lines do not mean that POs are unstable (on the contrary, the AS2 is the stable branch of the CS0). We use broken lines to distinguish the new types of motion. From now on, the AS1 and CS1 families are denoted by solid lines and the AS2 and CS2 by dashed lines.

Hence, for the mass combination (16,18 − 18), the AS1 starts from the minimum of the potential but because of the crossing (at about 0.9 eV) with the AS2, the center-saddle bifurcation CS2 emanates at lower energies than the CS1.

The CB diagram for the ozone isotopomer (18,16 − 16) is shown in Figure 12c. In this case, the AS2 starts at low energies, but because of the crossing with the AS1 at about 0.9 eV, the center-saddle bifurcation which emerges first is the CS1. As we can see from the plots of POs, the morphologies do not change by the different isotope combination. If we make the assignment to local bonds again, the low frequency AS2 is associated with the 18 − 16 oscillator and the AS1 with the 16 − 16 bond for energies below 0.9 eV. Indeed, at low energies, the AS1 branch of the (18,16 − 16) isotopomer coincides with the AS1 of the symmetric molecule (16,16 − 16). Above the crossing point, the morphologies of AS1 and AS2 are exchanged and the AS2 POs localize the motion in the *r* bond.

It is important to note that the (16,16 − 18) isotopomer is equivalent to the (18,16 − 16), and therefore, we expect its bifurcation diagram to be exactly the same, but reversing the role of local modes, AS1 and AS2, and center-saddle bifurcations CS1 and CS2. Now, the low frequency AS1 is associated to the local bond 16 − 18 and the high frequency AS2 to the 16 − 16 bond, of course, before the crossing. Because of the crossing of the two curves, the CS2 center-saddle bifurcation appears first. Keep in mind that the (18,16 − 16) case has the lowest association rate and the (16,16 − 18) the second highest.

From the above analysis of continuation/bifurcation diagrams, we expect that the symmetry does play a role in association/dissociation of ozone. We have shown that by breaking the symmetry of ozone with isotopic substitution, we generate a center-saddle bifurcation (CS0) and new types of states (AS2) are born. They go above the dissociation threshold and continue with the CS2 center-saddle bifurcation. These states lead to excitation of the diatomic molecule bond length *r*, and above the threshold, energies can be assigned to long lived resonances. An immediate association of these conclusions with the isotopic ozone effect is not easy, since the calculations up to now are for total angular momentum $J = 0$. How the resonances evolve with higher *J* values it worth studying.

5.2.2. Excited State $O_3(1^1B_2)$

Ozone is an important molecule for atmospheric chemistry because of its role in shielding the earth from harmful UV light. There have been numerous studies of its spectroscopy and photodissociation.[207] The absorption of the UV radiation excites electronically the molecule to the (1^1B_2) state. Recently, we have carried out theoretical *ab initio* calculations and we have shown that the two absorption bands

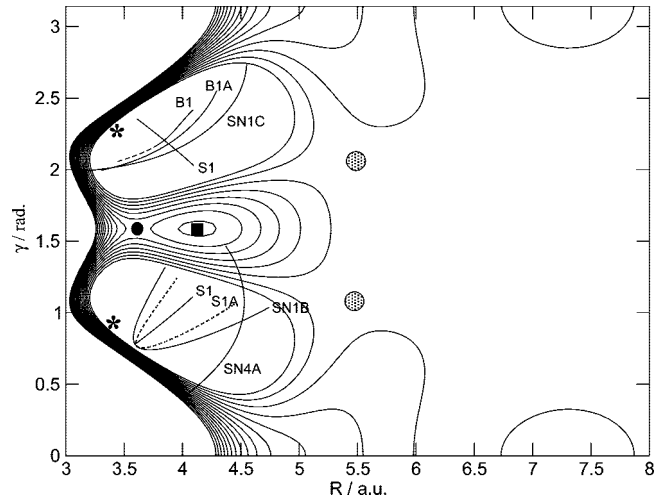

Figure 13. Potential energy contours for the diabatic $^1B_2$-state of ozone with periodic orbit plots. Energies are in electronvolts, distances in Bohrs, and the angle in radians. The energies cover the interval of (4.0−4.5) eV in 0.033 eV steps. The points shown on the graph mark the saddle points 1 (dotted circle), 2 (stars), 3 (filled circle), and 4 (filled square). Reprinted with permission from ref 147. Copyright 2006 World Scientific Publishing Company.

observed, Huggins and Hartley, are due to the excitation of the molecule from the ground electronic state to the (1^1B_2) state.[97] The mechanism of the photodissociation of ozone is complicated because of the involvement of several excited states.[208] Nevertheless, the construction of an analytical function for the diabatic (1^1B_2) state of ozone, as well as the calculation of high quality quantum mechanical vibrational eigenfunctions up to the dissociation threshold, as a result of the previous studies, lead us to investigate further the dynamics of the molecule in this excited state. The structure of phase space, and, thus, reaction paths on this surface, has been explored by the periodic orbits technique.[147]

The potential energy for the diabatic $^1B_2$-state of ozone has been described in detail in ref 97. The equilibrium geometry of ozone in this excited state has C_s symmetry, with one *long bond* and one *short bond*, in contrast to the case of the ground electronic state, where the minimum is of C_{2v} symmetry with two equal bonds. Because of the permutation symmetry of the molecule, there are three equivalent minima and several saddle points among them. The nuclear configurations are described in Jacobi coordinates, which are the distance *R* of the *long-bond* oxygen atom from the center of mass of the *short-bond* end atoms whose bond length is *r*, and the angle γ between the vectors $\vec{R}$ and $\vec{r}$. This Jacobi coordinate system is appropriate to describe the dissociation of a triatomic molecule.

All quantum mechanical calculations were performed with zero total angular momentum. The discrete variable representation[109] (DVR) was used to represent the Hamiltonian matrix. Two types of calculations have been performed: filter diagonalization[209] and harmonic inversion.[210] More details are given in ref 98.

In Figure 13 isopotential curves are depicted in the (R,γ) plane. The symbols on this picture mark the positions of the saddle points. The saddle points which separate two equivalent minima by exchanging their short and long bonds are denoted by stars. The geometry of this saddle is better portrayed in projections of the potential function in the plane with the two bond lengths of the molecule as coordinates shown in Figure 1 of ref 98. Note the differences in the

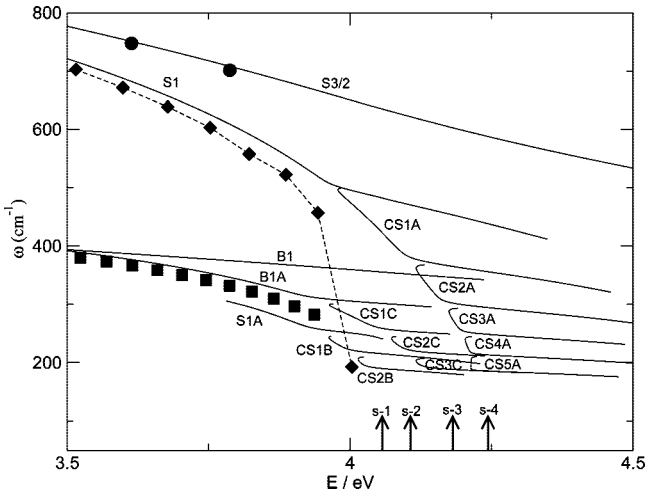

Figure 14. Continuation/bifurcation diagram of the $^1B_2$-state of ozone. S1 denotes the *long-bond* mode, S1A its double period bifurcation, S3 the *short-bond* mode, B1 the bend mode, and B1A an early center-saddle bifurcation of B1. The symbol CS denotes cascades of center-saddle bifurcations. CSiA is related with the S1 family, CSiB with the S1A family, and CSiC with the B1A family. The arrows mark the energies of the saddle points (s-*i*) in the potential. PO families related with the s-2 have not been located. Reprinted with permission from ref 98. Copyright 2004 American Institute of Physics.

values of *r* for the saddle points. Except for saddle-4, which is of second order (i.e., it has two unstable directions with imaginary frequencies), all the other saddles are of first order. The stable degree of freedom for saddle-4 is the *short-bond r*, as can be seen in Figure 13, where this saddle point appears as a maximum.

The normal-mode frequencies are estimated to be $\omega_3 = 1585$ cm^{-1} for the *short-bond* local mode, $\omega_1 = 743$ cm^{-1} for the *long-bond* local mode, and $\omega_2 = 400$ cm^{-1} for the bend. They are in an approximate $\omega_2:\omega_1:\omega_3 = 1:2:4$ resonance.

The evolution of the normal-mode frequencies with increasing energy is represented in the continuation/bifurcation diagram (Figure 14). In this figure, the three principal families of periodic orbits are shown and they are denoted as S1 for the *long-bond* stretch, B1 for the bend, and S3 for the *short-bond* stretch. B1 exhibits an early center-saddle bifurcation, B1A, at about 3.475 eV with a tiny energy gap, whereas a double period bifurcation is found for the S1 (S1A) at about 3.78 eV. As we can see in this figure, the three most anharmonic families, S1, S1A, and B1A, develop cascades of center-saddle bifurcations as energy approaches the dissociation limit (saddle-1) for the CSiB, the saddle-3 for the CSiC cascade, and saddle-4 for the CSiA, respectively. We have not searched for the PO which point to saddle-2. The center-saddle bifurcations are of similar type as found in the model quartic potential (Table 1). The frequency of the parent family levels off as energy approaches the critical energy of bifurcation, whereas new POs appear after the bifurcation. The whole scenario is repeated at higher energies, resulting in a cascade of such CS bifurcations. The stability of POs in this bifurcation diagram is not shown. In most cases, the anharmonic branch is stable, at least for some energy, and the other branch is unstable, and therefore, it is difficult to continue in energy. However, for a three-dimensional system, such as ozone, a CS bifurcation may show one single unstable and one double unstable branch instead. For larger molecules with more degrees of freedom, the number of combinations, of course, increases.

In Figure 14 the point symbols denote the quantum mechanical frequencies obtained from the energy differences of adjacent eigenstates whose wave functions can be clearly assigned. They are state overtone progressions of the short-bond stretch (S3), bend (B1A), and long-bond stretch (S1). The corresponding eigenfunctions have well recognized nodal structures, and therefore, the number of quanta in each mode can easily be assigned as $(0,0,n_3)$ for the S3 states, $(0,n_2,0)$ for B1A, and $(n_1,0,0)$ for the S1 states. In order to approximately account for the zero-point energy, the quantum results are shifted to lower energies by the zero-point energy. The energy differences are plotted with respect to the upper level. More details are given in ref 147.

6. Polyatomic Molecules

6.1. Acetylene

A molecule that has retained the interest of spectroscopists for decades is acetylene,[21,22] particularly the problem of the isomerization of acetylene to vinylidene.[211] Contrary to acetylene, for which numerous spectroscopic studies exist, its isomer vinylidene has not been identified unequivocally, although its existence is strongly supported by theoretical calculations. The 6D quantum mechanical calculations of Zou and Bowman[55] for this four atom system reveal the difficulties in obtaining accurate eigenfunctions and eigenenergies at high vibrational states. Most of the quantum mechanical investigations in the past were restricted to planar configurations of the molecule with four or five degrees of freedom, and only relatively recently were the acetylene vibrations investigated with full dimensional quantum mechanics.[212−214] Zou and Bowman[215] extended these calculations at such energies where isomerization of acetylene could be studied. In this work, the authors use a new full dimensional potential energy surface,[216,217] which predicts a smaller barrier to isomerization than an older version produced by Carter et al.[86,218] More recently, several groups have reported more accurate quantum studies of the acetylene−vinylidene system.[219,220]

Concerning the spectroscopy of acetylene, Jacobson et al.[21−23] studied dispersed fluorescence spectra in the energy region around 15000 cm^{-1}. This energy is close to the vinylidene minimum. By fitting the spectroscopically assigned levels of the *trans* and *cis* bending modes to an effective Hamiltonian, Jacobson et al. were able to show normal to local mode transitions. In a companion paper, a semiclassical analysis was presented for this two-dimensional effective Hamiltonian.[221] Although stretching normal to local mode transitions are known[80] and the asymmetric stretch of acetylene does show such a transition, it was rather surprising to find a similar bifurcation phenomenon for the bending modes. Specifically, the *trans* bending normal mode exhibits a local one, whereas the *cis* bending normal mode turns to a counter-rotation for the two hydrogen atoms;[221,23] that is, the two hydrogen atoms execute rotations around the CC bond in opposite directions. This normal-to-local transition was observed in the full quantum studies of acetylene vibration on a spectroscopically accurate force field.[214]

An early periodic orbit analysis of the principal and bifurcating families of acetylene was presented by Prosmiti and Farantos using a 6D potential function.[84] However, most

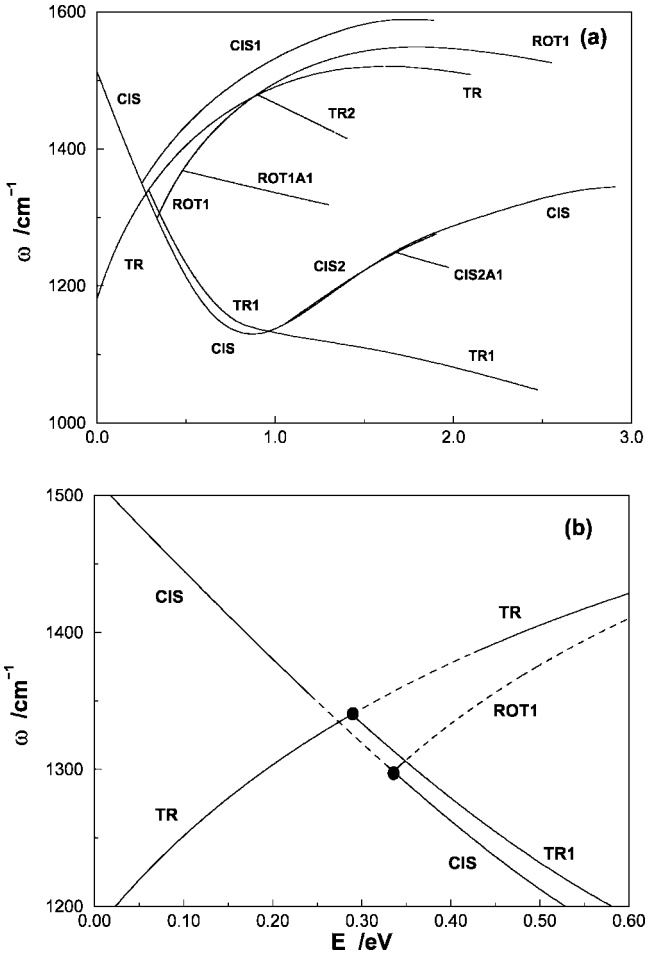

Figure 15. Continuation/bifurcation diagram of acetylene: (a) the two bending *trans* (TR) and *cis* (CIS) modes and (b) magnification of the *trans* and *cis* bending bifurcation diagram. In part b, solid lines indicate stable POs and dashed lines unstable ones. Reprinted with permission from ref 85. Copyright 2003 American Institute of Physics.

of the families located in this study were restricted in the plane, and thus, periodic orbits that come out of the plane, such as the counter-rotation, were not sought for. In a more recent publication,[85] we revisited the problem of the POs of acetylene by using a potential energy function which was a refinement of the Carter et al.[86] potential based on the accurate *ab initio* calculations of Stanton and Gauss.[216,217] The more pronounced difference between the two functions is the height of the barrier to isomerization of vinylidene to acetylene. In the old version, the barrier's height is 0.373 eV, while in the new one it is 0.107 eV. The energy of the vinylidene minimum has also changed. Relative to the acetylene minimum, it is 1.735 eV in the Carter et al. potential and 1.991 eV in the new function. The location of POs has been done in a Cartesian coordinate system with twelve degrees of freedom. The momenta were adjusted to ensure zero total angular momentum. However, we obtained plots of the trajectories in the diatom−diatom (CH−CH) coordinate system. Newton−Raphson multiple shooting techniques to find the periodic orbits[162] were employed.

Figure 15a contains the continuation/bifurcation diagram of the *cis* and *trans* bending families, whereas a magnification of it is depicted in Figure 15b. For comparison with the work of Jacobson et al.,[23] where the even quantum number bending states are assigned, we have multiplied the frequencies by two. The *trans* family shows a pitchfork bifurcation at the energy of 0.289 eV, with the new families remaining stable for most energies. The TR family becomes stable again at 0.42 eV. By projecting the trajectory in the (θ_1,θ_2) plane, we find the bifurcating TR1 POs almost parallel to one of the angles, thus showing their local character. The stability of the bifurcating periodic orbits (TR1) means that the region of phase space around them is less chaotic, and this explains the remark of Jacobson et al.[23] that the spectrum becomes less complex at higher energies.

For the *cis* bending principal family, it was initially located in an out of plane periodic orbit at the energy 0.253 eV, CIS1. However, the counter-rotation periodic orbits emerge at the energy of 0.335 eV, ROT1. We see that the CIS family has turned to unstable at 0.252 eV, and it becomes stable again at the bifurcation energy of ROT1. The counter-rotation POs are unstable.

Comparing Figure 15b with the two-dimensional quantum results shown in Figure 7 of the Jacobson et al.[23] article, we see that the bifurcation analysis of periodic orbits on the global potential energy surface correctly predicts that, first, the bifurcation of the *trans* mode (TR1) occurs at a lower energy than the bifurcation of the *cis* mode (ROT1). Second, the counter-rotation has a negative anharmonicity and the TR1 a positive anharmonicity. However, while the continuation lines cross in Figure 15b, the quantum mechanical results show an avoided crossing. Even correcting with the ZPE, it was not possible to bring classical and quantum pictures into agreement, which means that the global potential function does not predict the bending energy levels accurately in this region of the spectrum.

There have been several studies on the acetylene vibrational spectrum[139,222−224] that predict the counter-rotation periodic orbits. In their very recent work, Jung and Taylor[60] managed to unequivocally assign all 144 eigenstates of polyad 22. By *lifting* the semiclassical wave functions from the 2D reduced dimension space to the Cartesian displacement coordinates, they identified the classical organizing points which are a minimum, a saddle, and a maximum. As a result, the polyad states are classified in three classes: local bend (minimum), cross bend (saddle), and counter-rotor (maximum).

The periodic orbit analysis of the 6D *global* PES reveals more details and bifurcations than the 2D effective Hamiltonian. However, it is remarkable that two totally different approaches, different coordinates and Hamiltonian forms, unveil the basic dynamics of this four atom molecule at relatively high vibrational energies. Not only the relevant periodic orbits are predicted but even their stability. This is an important conclusion if we take into account that as the size of a molecule increases the construction of accurate potential functions becomes a remote target for computational chemistry.

Other tetraatomic molecules studied by dispersed fluorescence and stimulated emission pumping spectroscopies are HFCO[32,33] and thiophosgene.[39,225] For the latter ($SCCl_2$), a spectroscopic Hamiltonian was produced by van Vleck perturbation theory and analyzed by visual inspection of the 3D reduced dimension wave functions.[135] Vibrational levels up to 9000 cm^{-1} were assigned, revealing the regularity and localization of these highly excited states. Very recent work by Chowdary and Gruebele[39,226] demonstrates sharp features in the vibrational spectrum of $SCCl_2$ at and above its two lowest-lying dissociation limits. Highly regular vibrational progressions persist at dissociation, as was seen in some

smaller molecules. Nearly all of the studied transitions could be assigned and fitted by a simple effective Hamiltonian without resonance terms, up to a total vibrational excitation of 36 quanta. The character of the highly excited vibrational wave functions is not normal modelike, but it nonetheless arises gradually from the normal modes as the energy increases. As a matter of fact, looking at the plots of the eigenfunctions[39] calculated in the normal coordinates of the C−S bond stretch (q_1) and the out of plane bend (q_4), one can recognize the trace of a 1:2 resonance ($\omega_4:\omega_1 = 1:2$) at low energies and the assignment of the high energy levels to a bifurcating family of periodic orbits.

Larger molecules such as CHBrClF,[60] CDBrClF, and CF_3CHFI,[61,60] studied by effective 3D Hamiltonians which accurately fit Fourier transform infrared spectra, show localization in configuration space and regularity at highly excited energies. This is counterintuitive, since as the number of normal modes increases in polyatomic molecules, one expects overlapping resonances and, thus, chaos in the vibrational motions of the molecule. Are the studied molecules exceptional or is the observed localization more common among polyatomic molecules? This question is pertinent to biomolecules, since we do expect regularities. In refs 39 and 226, the authors argue that the fraction of states partly localized in state space at the dissociation energy increases with the number of vibrational modes; the same energy is distributed over more modes, resulting in fewer quanta per mode, i.e. more states at the edge, and hence fewer coupling partners nearby in state space and smaller anharmonic couplings. Although this is true, we should however not forget that as the number of vibrational degrees of freedom increases we expect more overlapping resonances which result in chaos even at low energies. In the next section we present our first efforts to investigate the above question.

6.2. Biomolecules

Biomolecules are complex systems, and therefore, it is not surprising that statistical mechanical methods are used for their study. The systematic methods of nonlinear mechanics based on hierarchically calculating stationary objects such as periodic orbits, tori, and stable and unstable manifolds are taken into account only for systems with a few degrees of freedom. However, we argued before that periodic orbits offer the means to extract the physics from complicated calculations and even to get reliable estimates of quantum energies. Recently, it has been demonstrated that periodic orbits can be located for biomolecules such as the dipeptide of alanine, a molecule with sixty internal degrees of freedom.[103]

Alanine dipeptide has served as a prototype molecule for testing new algorithms in numerous studies in the past.[227,228] We also used this molecule by employing the parameters of CHARMM27 for the force field,[101] Morse functions for the bond stretches, and harmonic potentials for the angles. In this work, the principal families emanating from the two lowest minima (*min*1 and *min*2) and the transition state (*ts*1) between them (see Figure 16) were investigated. The energy barrier for the lowest conformation *min*1 to isomerize to *min*2 is approximately 0.6 kcal/mol, and the geometries of the two stable conformers are those shown in Figure 16. They differ in the orientation of one oxygen. The geometries of these two conformations correspond to a folded (absolute minimum) and to an elongated structure, respectively. Therefore,

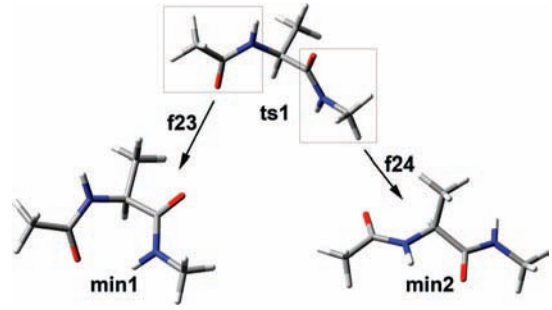

Figure 16. Geometries of the two minima and the transition state for the lowest energy isomerization reaction of alanine dipeptide. The two squares drawn on the transition state enclose the atoms which execute the largest motions in the *f*23 (left) and *f*24 (right) periodic orbits. Quenching the energy from configurations of the *f*23 and *f*24 periodic orbits specifically leads to the minima *min*1 and *min*2, respectively. From left to right, the balls correspond to the atoms of the chemical structure $CH_3CONHCH(CH_3)CONHCH_3$. Reprinted with permission from ref 103. Copyright 2007 American Institute of Physics.

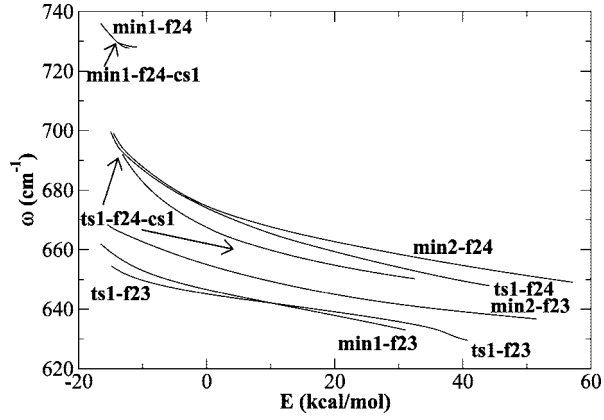

Figure 17. Continuation/bifurcation diagrams of the principal families of periodic orbits *f*23 and *f*24 originated from the equilibria *min*1 and *min*2 and the saddle point *ts*1 of alanine dipeptide. Reprinted with permission from ref 103. Copyright 2007 American Institute of Physics.

we use the distance of the two nitrogen atoms to assign trajectories trapped in one or the other minimum.

Among the sixty vibrational normal modes, the 23rd and 24th were studied. The numbers used to assign the families are the same as the enumeration of the harmonic normal modes, i.e., by increasing frequency. The 23rd and 24th normal modes have approximately localized motions. The NH and CO bonds oscillate in phase, executing the largest displacements. Our interest in these particular normal modes came from their specificity. Starting with initial configurations from these oscillations and minimizing the energy, we approach a specific minimum, the *f*23 mode leads to *min*1, and the *f*24 leads to *min*2 (Figure 16).

In Figure 17 the continuation/bifurcation (CB) diagram for the *f*23 and *f*24 families coming out from the three equilibria of the molecule (*min*1, *min*2, *ts*1) is shown. The principal families generated from the minima are initially stable. The periodic orbits which emerge from the transition state start as unstable with the same rank of instability as the transition state. *ts*1 has rank-1 instability. In this figure, the frequency obtained from the period of PO as a function of the total energy of the molecule is plotted. The anharmonic behavior of these vibrational modes is evident. For the *f*24 families of *min*1 and the saddle point (*ts*1), an early center-saddle bifurcation is observed. This means that at a specific

energy the continuation line levels off, decreasing its anharmonicity, and a new pair of families of periodic orbits emerges, one of them with stable periodic orbits and the other with unstable ones. The mechanism of appearance of these bifurcations is the same as was described before.[147] It is worth noting the higher frequency of the 24th mode of *min*1 compared to the other two equilibrium points of the potential function. After the appearance of the center-saddle bifurcation (family *min*1 − *f*24 − *cs*1), it was very difficult to continue this branch at higher energies. We expect a cascade of center-saddle bifurcations as we go up in energy.[9−11]

To the best of our knowledge, this molecule is the first which demonstrates that principal families with high anharmonicity can indeed be located for a rather extended energy interval (≈3 eV) from different minima and transition states of a large molecule. New periodic orbits emanate from CS bifurcations, as it was repeatedly found in triatomic molecules.

The question of what happens to a polypeptide in water solution has been addressed by several investigators.[229,230] We have also examined the stability of the *min*1 conformation excited to the normal mode *f*23, for example, when it is embedded in water.[231] This is done by choosing initial conditions for the coordinates and velocities of the alanine dipeptide atoms along the periodic orbits of a specific isomer and normal mode. Then, we combine them with the coordinates and velocities of 487 water molecules, described by the TIP3P parameters. These embedded states simulate the excitation of alanine dipeptide in an overtone state. After that, the dynamics is followed for 50 ps in a canonical ensemble at several temperatures.

Localization in complex systems is currently a subject of intense research.[52,232] For example, energy localization and the theory of breathers have been utilized to argue for the existence of long, nonexponential excited state relaxation in myoglobin.[232] In these studies, the authors used simple models to argue that localized states may be responsible for the observed long relaxation times. The existence of stable periodic orbits for substantial energy ranges in alanine dipeptide described with an empirical potential function supports these arguments. Such potentials are widely used in simulations of biomolecules. Systematic investigations of the problem of nonexponential relaxation in polyatomic molecules have been presented by Gruebele.[233,234]

Different time scales in the isomerization process of alanine dipeptide depending on the excitation of specific vibrational modes but from different conformations[103] have been found. Although we excite similar modes in the three conformations (*min*1, *min*2, *ts*1), their subsequent dynamics differ substantially. Novel spectroscopic methods have been applied to study small peptides in the subpicosecond time scale. In a recent investigation of alanine tripeptide in water by two-dimensional vibrational spectroscopy, conformational fluctuations at the time scale of 0.1 ps have been reported.[235] It is worth noting that the stability parameter of the unstable POs which originates from the transition state *ts*1 gives an upper estimate of the lifetime of the complex. In the case of alanine dipeptide, this time is predicted to be 0.3 ps, close to that found by Hamm and co-workers.[235]

Complexity is inherent in biological molecules not only because of the large number of atoms but also because of their nonlinear interactions responsible for chaotic behaviors, resonances, and bifurcation phenomena. Thus, versatile spectroscopic techniques have been invented to achieve temporal and spatial resolution[5,46,236] to minimize the uncertainties in assigning the spectra of complex molecules. Can we associate spectral lines to specific chemical bonds or species in a large molecule? Can energy stay localized in a bond for a period of time sufficiently long to leave a fingerprint in the spectrum? These long-standing problems were investigated by studying the resonance Raman spectra of ferryl-oxo intermediates of cytochrome *c* oxidase.

Cytochrome *c* oxidase (C*c*O) couples the four electron reduction of dioxygen to water with the pump of four protons across the inner mitochondrial membrane contributing to the electrochemical gradient that is used to synthesize ATP. Electrons from cytochrome *c* pass through a heme-a group and are then transferred to the binuclear heme-a_3/Cu_B active site where dioxygen is reduced. The understanding of the mechanism of action of C*c*O has been a matter of considerable debate. In the reaction of the enzyme with O_2, the O−O bond is cleaved, producing the ferryl-oxo (Fe^{IV}═O) species. In the reaction of the fully reduced enzyme with O_2, either two peaks are identified in the spectra exhibiting ferryl-oxo character with (Fe−O) frequency at 790 and 804 cm^{-1} or only the latter. It is clear that establishing the dynamics of the protein environment adjacent to the active site subsequent to O−O bond cleavage is essential first in understanding the linkage of oxygen activation with proton translocation and second in assigning the 790/804 cm^{-1} peaks.

An application of the periodic orbits method for the active site of the enzyme with 95-atoms has recently been published, in conjunction with molecular dynamics calculations of larger systems which include the embraced active site by the protein and selected protonated/deprotonated conformations of amino acids.[104] It was demonstrated that for the active site stable periodic orbits exist for a substantial energy range. Families of periodic orbits which are associated with the vibrations of the Fe^{IV}═O bond mark the regions of phase space where nearby trajectories remain localized, and they enable one to assign the spectral bands of the active site in the protein matrix. It has also been demonstrated that proton motion adjacent to an active site can lead to significant perturbations of the Fe^{IV}═O isotopic difference vibrational spectra in cytochrome *c* oxidase, without a change in the oxidation state of the metal sites. This finding links spectroscopic characteristics to protonation events occurring during enzymatic turnover.[104]

In Figure 18, the CB diagram is shown for those principal families that are mainly associated with the ferryl-oxo bond oscillations. The labels correspond to the harmonic normal modes from which the family originates. We can see three major frequency regions. The low frequency f134 family corresponds to a breathing mode of the imidazole in the proximal area of iron. The f139 family is associated with an oscillation of the Fe−N bond, but it appears to be highly anharmonic. This anharmonicity results in a center-saddle bifurcation, cs139a.

The f139 family of POs is an example of how anharmonicity and coupling to other degrees of freedom can drastically change the harmonic vibrational frequency of the mode even with a small increase in energy. Thus, we expect and do find changes in the spectra of the larger system by examining the different protonation states which affect the electrostatic environment of the Fe−O bond.[104] Unfortunately, it is difficult to foresee such nonlinear phenomena in advance. Usually, spectroscopic investigations or detailed calculations are required.

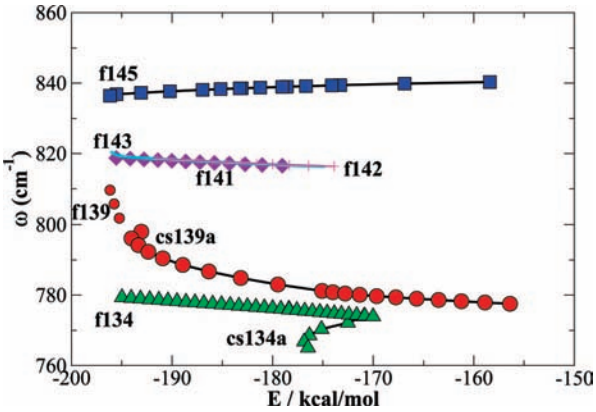

Figure 18. Continuation/bifurcation diagram of the active site of ferryl-oxo intermediate of Cytochrome *c* Oxidase, which depicts the evolution of the frequencies in a few families of periodic orbits with increasing total energy. These families are mainly associated with the Fe═O bond oscillations. CS denotes center-saddle bifurcations. Reprinted with permission from ref 104. Copyright 2008 American Chemical Society.

The middle frequency families, f141, f142, and f143, differ only by a few wavenumbers and show small anharmonicities. They involve oscillations of Fe with the porphyrin ring. The higher frequency periodic orbits of the f145 family show negative anharmonicity and represent asymmetric oscillations of the imidazole−Fe═O bonds. In all these families, the hydroxyl group attached to Cu_B shows appreciable displacements.

In principle, one could examine all vibrational modes of the active site and foresee the spectroscopic properties and dynamics of the species. Practically, we concentrate on those features which are related to experimental observations. Questions concerning the reliability of the potential function are of course serious as far as quantitative answers are concerned. However, as was stated before, the nonlinear properties of motion show structural stability and we do not expect them to change drastically when improving the potential function.

7. Conclusions

The question of statistical or nonstatistical dynamical behavior of large systems with many degrees of freedom has a long history. The early numerical experiments of Fermi, Pasta, Ulam, and Mary Tsingou (FPU)[237−239] on nonlinear vibrating strings demonstrated that large systems not necessarily exhibit ergodic behavior as was expected, but instead quasi-periodic motions. The latter implies localization of the energy in a few vibrational modes. In spite of these early results, the statistical RRKM theory[190] for calculating reaction rate constants has been very popular for decades with numerous applications. The FPU calculations[237] were important in showing both the complexity of nonlinear system behavior and the value of computer simulation in analyzing these systems.

Polyatomic molecules vibrationally excited at energies close to the isomerization or dissociation energies are nonlinear systems, and they are expected to show all these nonlinear phenomena extensively studied in the last decades. Modern spectroscopy reveals the fingerprints of these phenomena in the spectra: sharp spectral lines attributed to vibrational states localized in configuration space, resonances between normal modes or bifurcations of them, and chaotic behaviors with specific spectral distributions.[181] It is true that, in spite of all these studies, even now the discovery of sharp spectral lines or nonexponential decays in polyatomic molecules brings a surprise to the investigators, and the pertinent quantum states are named *exotic*.

In this review we have demonstrated that the spectral assignment of vibrationally excited molecules does require the identification of those classical stationary objects (equilibria−periodic orbits−tori−manifolds) that act as *organizing structures*[60] for the quantum mechanical eigenstates. Hence, as we explore in the first level the landscape of the PES of polyatomic molecules for anticipating molecular dynamics, at the second level periodic orbits analysis is necessary to explore molecular dynamics in detail. A nice application of a PO analysis was recently presented on the study of the dissociation mechanism in bichromatically driven diatomic molecules.[240] Through the stability of periodic orbits, the investigators analyze the dissociation probability when parameters, such as the two amplitudes and the phase lag of the laser field, are varied.

Bifurcation analysis of periodic orbits which emanate from the saddle points of polyatomic PESs may also be useful in studying the bifurcations of the no-return transition states (NHIM), as a recent study has shown.[241] Although periodic orbits for systems with three and higher degrees of freedom do not separate the phase space into two disjoined sets of reactants and products, the reduced dimension tori around the unstable POs may guide one to predict possible bifurcations of NHIM at high energies. We have constructed continuation/bifurcation diagrams of periodic orbits that emanate from saddle points of the PES for FH_2[170] and recently for alanine dipeptide.[103]

Recognizing that the transition from normal to local stretch or bend modes as the energy of the molecule varies is the result of a pitchfork bifurcation, we understand that localization may result because of other types of bifurcations as well, more commonly center-saddle. By establishing a correspondence between quantum eigenstates and phase space structures, we open a channel to control the dynamics of polyatomic molecules.[242]

In this review it is demonstrated that we do have the means for locating POs in large molecules with many degrees of freedom in Cartesian coordinates, revealing a lot of the details in bifurcations and thus nonlinear dynamics of the molecule. Nevertheless, since nature very often simplifies our work by reducing the active space of resonances in two or three dimensions, effective Hamiltonians and well established semiclassical theory assist us to assign complex spectra and extract the dynamics not only of overtone states but also of combination states, too.

It is true that, even after decades of research in molecular spectroscopy, there are not many spectroscopic studies of polyatomic molecules at energies close to and above isomerization or dissociation energies. Apparently, this is due to their complexity. We believe that the application of nonlinear molecular mechanics will accelerate the investigation of highly excited molecules. Moreover, we do foresee the discovery of new phenomena, such as complex instability,[149] to be observed spectroscopically in polyatomic molecules.

8. Acknowledgments

We are grateful to Dr. Sergy Grebenshchikov for the valuable contributions and assistance he offered to us over the past years. We thank Prof. Srihari Keshavamurthy for sending us his article (ref 61) prior to publication. Financial support from the European Union ToK grant GRID-COM-

PCHEM (MTKD-CT-2005-029583) is kindly acknowledged. H.G. acknowledges financial support from the U.S. Department of Energy (No. DE-FG02-05ER15694).

9. References

(1) Levine, R. D.; Berstein, R. B. *Molecular Reaction Dynamics and Chemical Reactivity*, 3rd ed.; Oxford University Press: New York, 1987.
(2) Crim, F. F. *Proc. Natl. Acad. Sci. U.S.A.* **2008**, *105*, 12654–12661.
(3) Liu, Z.; Feldman, L. C.; Tolk, N. H.; Zhang, Z.; Cohen, P. I. *Science* **2006**, *312*, 1024–1026.
(4) Tully, J. C. *Science* **2006**, *312*, 1004–1005.
(5) Dai, H.-L.; Field, R. Molecular Dynamics and Spectroscopy by Stimulated Emission Pumping; *Advanced Series in Physical Chemistry*; World Scientific Publishing Company: Singapore, 1995.
(6) Guckenheimer, J.; Holmes, P. *Nonlinear Oscillations, Dynamical Systems, and Bifurcations of Vector Fields*, 2nd ed.; Springer-Verlag: New York, 1990; Vol. 42.
(7) Wiggins, S. *Introduction to Applied Nonlinear Dynamical Systems and Chaos*; Springer-Verlag: New York, 1990.
(8) Poincaré, H. *New Methods of Celestial Mechanics*; Springer-Verlag: New York, 1992; Vol. 13.
(9) Ishikawa, H.; Field, R. W.; Farantos, S. C.; Joyeux, M.; Koput, J.; Beck, C.; Schinke, R. *Annual Review of Physical Chemistry*; Annual Reviews: Palo Alto, CA, 1999; Vol. 50, pp 443−484.
(10) Joyeux, M.; Farantos, S. C.; Schinke, R. *J. Phys. Chem.* **2002**, *106*, 5407–5421.
(11) Joyeux, M.; Grebenshchikov, S. Y.; Bredenbeck, J.; Schinke, R.; Farantos, S. C. *Adv. Chem. Phys.* **2005**, *130*, 267–303.
(12) Brown, R. C.; Wyatt, R. E. *Phys. Rev. Lett.* **1986**, *57*, 1–4.
(13) Brown, R. C.; Wyatt, R. E. *J. Phys. Chem.* **1986**, *90*, 3590–3594.
(14) Wiggins, S. *Normally Hyperbolic Invariant Manifolds in Dynamical Systems*; Springer-Verlag: New York, 1994.
(15) Wiggins, S.; Wiesenfeld, L.; Jaffé, C.; Uzer, T. *Phys. Rev. Lett.* **2001**, *86*, 5478–5481.
(16) Uzer, T.; Jaffé, C.; Palacián, J.; Yanguas, P.; Wiggins, S. *Nonlinearity* **2002**, *15*, 957–992.
(17) Waalkens, H.; Schubert, R.; Wiggins, S. *Nonlinearity* **2008**, *21*, R1−R118.
(18) Child, M. S. *Semiclassical Mechanics with Molecular Applications*; Oxford University Press: Cary, NC, 1991.
(19) Gutzwiller, M. C. *Chaos in classical and quantum mechanics*; Springer-Verlag: New York, 1990; Vol. 1.
(20) Miller, W. H. *J. Phys. Chem. A* **2001**, *105*, 2942–2955.
(21) Jacobson, M. P.; O'Brien, J. P.; Silbey, R. J.; Field, R. W. *J. Chem. Phys.* **1998**, *109*, 121–123.
(22) Jacobson, M. P.; O'Brien, J. P.; Field, R. W. *J. Chem. Phys.* **1998**, *109*, 3831–3840.
(23) Jacobson, M. P.; Silbey, R. J.; Field, R. W. *J. Chem. Phys.* **1999**, *110*, 845–859.
(24) Jung, C.; Taylor, H. S.; Jacobson, M. P. *J. Phys. Chem. A* **2001**, *105*, 681–693.
(25) Temsamani, M. A.; Herman, M.; Solina, S. A. B.; O'Brien, J. P.; Field, R. W. *J. Chem. Phys.* **1996**, *105*, 11357–11359.
(26) El Idrini, M.; Lievin, J.; Campargue, A.; Herman, M. *J. Chem. Phys.* **1999**, *110*, 2074–2086.
(27) Jonas, D. M.; Solina, S. A. B.; Rajaram, B.; Cohen, S. J.; Field, R. W.; Yamanouchi, K.; Tsuchiya, S. *J. Chem. Phys.* **1993**, *99*, 7350–7370.
(28) Ishikawa, H.; Nagao, C.; Mikami, N.; Field, R. *J. Chem. Phys.* **1998**, *109*, 492–503.
(29) Yamanouchi, K.; Takeuchi, S.; Tsuchiya, S. *J. Chem. Phys.* **1990**, *92*, 4044–4054.
(30) Yamanouchi, K.; Yamada, H.; Tsuchiya, S. *J. Chem. Phys.* **1988**, *88*, 4664–4670.
(31) Sako, T.; Yamanouchi, K. *Chem. Phys. Lett.* **1996**, *264*, 403–410.
(32) Choi, Y. S.; Moore, C. B. *J. Chem. Phys.* **1991**, *94*, 5414–5425.
(33) Yamamoto, T.; Kato, S. *J. Chem. Phys.* **1998**, *109*, 9783–9794.
(34) Tobiason, J. D.; Dunlop, J. R.; Rohlfing, E. A. *J. Chem. Phys.* **1995**, *103*, 1448–1469.
(35) Keller, H.-M.; Flöthmann, H.-M.; Dobbyn, A. J.; Schinke, R.; Werner, H.-J.; Bauer, C.; Rosmus, P. *J. Chem. Phys.* **1996**, *105*, 4983–5004.
(36) Keller, H.-M.; Stumpf, M.; Schröder, T.; Stöck, C.; Temps, F.; Schinke, R.; Werner, H.-J.; Bauer, C.; Rosmus, P. *J. Chem. Phys.* **1997**, *106*, 5359–5378.
(37) Northrup, F. J.; Bethardy, G. A.; Macdonald, R. G. *J. Mol. Spectrosc.* **1997**, *186*, 349–362.
(38) Delon, A.; Reiche, F.; Abel, B.; Grebenshchikov, S. Y.; Schinke, R. *J. Phys. Chem.* **2000**, *104*, 10374–10382.
(39) Chowdary, P. D.; Gruebele, M. *J. Chem. Phys.* **2009**, *130*, 024305.
(40) Henry, B. R. *Vibrational Spectra and Structure*; Elsevier: New York, 1993; Vol. 10.
(41) Crim, F. F. *Acc. Chem. Res.* **1999**, *32*, 877–884.
(42) Leitner, D. M. *Adv. Chem. Phys.* **2005**, *130*, 205–256.
(43) Leitner, D. M. *Annual Review Physical Chemistry*; Annual Reviews: Palo Alto, CA, 2008; Vol. 59, pp 233−259.
(44) Backus, E. H.; Nguyen, P. H.; Botan, V.; Pfister, R.; Moretto, A.; Crisma, M.; Toniolo, C.; Stock, G.; Hamm, P. *J. Phys. Chem. B* **2008**, *112*, 9091–9099.
(45) Kolano, C.; Helbing, J.; Sander, W.; Hamm, P. *J. Phys. Chem. B* **2008**, *111*, 11297–11302.
(46) Hamm, P.; Helbing, J.; Bredenbeck, J. *Annu. Rev. Phys. Chem.* **2008**, *59*, 291–317.
(47) Treuffet, J.; Kubarych, K. J.; Lambry, J.-C.; Pilet, E.; Masson, J.-B.; Martin, J.-L.; Vos, M. H.; Joffre, M.; Alexandrou, A. *Proc. Natl. Acad. Sci. U.S.A.* **2007**, *104*, 15705–15710.
(48) Koutsoupakis, C.; Pinakoulaki, W.; Stavrakakis, S.; Daskalakis, V.; Varotsis, C. *Biochim. Biophys. Acta* **2004**, *1655*, 347–352.
(49) Koutsoupakis, C.; Soulimane, T.; Varotsis, C. *Biophys. J.* **2004**, *86*, 2438–2444.
(50) Varotsis, C.; Babcock, G. T. *Biochemistry* **1990**, *29*, 7357–7362.
(51) Aubry, S. *Physica D* **1997**, *103*, 201–250.
(52) Campbell, D. K.; Flach, S.; Kivshar, Y. S. *Phys. Today* **2004**, *43*, 43–49.
(53) Sievers, A. J.; Takeno, S. *Phys. Rev. Lett.* **1988**, *61*, 970–973.
(54) Goldfield, E. M.; Gray, S. K. *Adv. Chem. Phys.* **2007**, *136*, 1–37.
(55) Zou, S.; Bowman, J. M. *J. Chem. Phys.* **2002**, *117*, 5507–5510.
(56) Kellman, M. E. *Annu. Rev. Phys. Chem.* **1995**, *46*, 395–422.
(57) Kellman, M. E.; Tyng, V. *Acc. Chem. Res.* **2007**, *40*, 243–250.
(58) Joyeux, M.; Sugny, D. *Can. J. Phys.* **2002**, *80*, 1459–1480.
(59) Joyeux, M.; Sugny, D.; Tyng, V.; Kellman, M.; Ishikawa, H.; Field, R. W.; Beck, C.; Schinke, R. *J. Chem. Phys.* **2000**, *112*, 4162–4172.
(60) Jung, C.; Taylor, H. S. *J. Phys. Chem. A* **2007**, *111*, 3047–3068.
(61) Manikandan, P.; Semparithi, A.; Keshavamurthy, S. *J. Phys. Chem. A* **2009**, *113*, 1717–1730.
(62) Landau, L. D.; Lifshitz, E. M. *Mechanics*, 3rd ed.; Pergamon Press: Oxford, England, 1976.
(63) Vleck, J. H. V. *Rev. Mod. Phys.* **1951**, *23*, 213–227.
(64) Birkhoff, G. D. *Colloq. Pub. No. 9* **1979**, 14–22.
(65) Gustavson, F. G. *Astron. J.* **1966**, *71*, 670–686.
(66) Farantos, S. C. *Int. Rev. Phys. Chem.* **1996**, *15*, 345–374.
(67) Montaldi, J.; Roberts, M.; Stewart, I. *Nonlinearity* **1990**, *3*, 695–730.
(68) Hanssmann, H. *Local and Semi-Local Bifurcations in Hamiltonian Dynamical Systems: Results and Examples*; Springer-Verlag: Berlin, Heidelberg, 2007.
(69) Main, J.; Mandelshtam, V. A.; Wunner, G.; Taylor, H. S. *Nonlinearity* **1998**, *11*, 1015–1035.
(70) Martens, C. C.; Davis, M. J.; Ezra, G. S. *Chem. Phys. Lett.* **1987**, *142*, 519–528.
(71) Engel, Y. M.; Levine, R. D. *Chem. Phys. Lett.* **1989**, *164*, 270–278.
(72) Heller, E. J. *Phys. Rev. Lett.* **1984**, *53*, 1515–1518.
(73) Polavieja, G.; Borondo, F.; Benito, R. M. *Phys. Rev. Lett.* **1994**, *73*, 1613–1616.
(74) Schweizer, W.; Jans, W.; Uzer, T. *Phys. Rev. A* **1998**, *58*, 1382–1388.
(75) Wales, D. J. *Energy Landscapes: Applications to Clusters, Biomolecules and Glasses*; Cambridge University Press: 2004.
(76) In this article we adopt the term center-saddle (CS) elementary bifurcation in accordance with mathematical literature for Hamiltonian systems,[68] instead of the term saddle-node (SN) used for generic dynamical systems and employed in our previous publications.
(77) Lawton, R. T.; Child, M. S. *Mol. Phys.* **1981**, *44*, 709–723.
(78) Prosmiti, R.; Farantos, S. C.; Guo, H. *Chem. Phys. Lett.* **1999**, *311*, 241–247.
(79) Herzberg, G. *Infrared and Raman Spectra*; Van Nostrand: New York, 1945.
(80) Halonen, L. *Adv. Chem. Phys.* **1998**, *104*, 41–179.
(81) Jensen, P. *Mol. Phys.* **2000**, *98*, 1253–1285.
(82) Keshavamurthy, S.; Ezra, G. S. *J. Chem. Phys.* **1997**, *107*, 156–179.
(83) Paskauskas, R.; Chandre, C.; Uzer, T. *Phys. Rev. Lett.* **2008**, *100*, 083001–4.
(84) Prosmiti, R.; Farantos, S. C. *J. Chem. Phys.* **1995**, *103*, 3299–3314.
(85) Prosmiti, R.; Farantos, S. C. *J. Chem. Phys.* **2003**, *118*, 8275–8280.
(86) Murrell, J. N.; Carter, S.; Farantos, S. C.; Huxley, P.; Varandas, A. J. C. *Molecular Potential Energy Functions*; John Wiley and Sons Ltd: 1984.
(87) Mezey, P. G. *Potential Energy Hypersurfaces*; Elsevier Science Publishers B.V.: Amsterdam, The Netherlands, 1987; Vol. 53.
(88) Collins, M. A. *Adv. Chem. Phys.* **1996**, *93*, 389–453.
(89) Werner, H.-J.; Knowles, P. J.; Lindh, R.; Manby, F. R.; Schütz, M.; et al. *MOLPRO, version 2008.1, a package of ab initio programs*; 2008.

(90) Ahlrichs, R.; Bär, M.; Häser, M.; Horn, H.; Kölmel, C. *Chem. Phys. Lett.* **1989**, *162*, 165–169.
(91) Ahlrichs, R.; et al. TURBOMOLE v5-8-0; 2005.
(92) Frisch, M. J.; Trucks, G. W.; Schlegel, H. B.; Scuseria, G. E.; Robb, M. A.; Cheeseman, J. R.; Montgomery, J. A., Jr.; Vreven, T.; Kudin, K. N.; Burant, J. C.; et al. *Gaussian03*; Gaussian Inc.: Wallingford, CT, 2003.
(93) Wang, S.; Hu, P.; Zhang, Y. *J. Phys. Chem. B* **2007**, *111*, 3758–3764.
(94) Laganá, A.; Riganelli, A. Reaction and Molecular Dynamics; *Lecture Notes in Chemistry*; Springer: 1999; Vol. 75.
(95) Ch. Beck, H.-M. K.; Grebenshchikov, S. Y.; Schinke, R.; Farantos, S. C.; Yamashita, K.; Morokuma, K. *J. Chem. Phys.* **1997**, *107*, 9818–9834.
(96) Stamatiadis, S.; Farantos, S. C.; Keller, H.-M.; Schinke, R. *Chem. Phys. Lett.* **2001**, *344*, 565–572.
(97) Qu, Z.; Zhu, H.; Tashiro, M.; Schinke, R.; Farantos, S. C. *J. Chem. Phys.* **2004**, *120*, 6811–6814.
(98) Qu, Z.; Zhu, H.; Schinke, R.; Farantos, S. C. *J. Chem. Phys.* **2004**, *121*, 11731–11745.
(99) Siebert, R.; Fleurat-Lessard, P.; Schinke, R.; Bittererová, M.; Farantos, S. C. *J. Chem. Phys.* **2002**, *116*, 9749–9767.
(100) Wang, J.; Cieplak, P.; Kollman, P. A. *J. Comput. Chem.* **2000**, *21*, 1049–1074.
(101) Foloppe, N.; MacKerell, A. D. *J. Comput. Chem.* **2000**, *21*, 86–104.
(102) Rapaport, D. C. *The Art of Molecular Dynamics Simulation*; Cambridge University Press: 1995.
(103) Farantos, S. C. *J. Chem. Phys.* **2007**, *126*, 175101–175107.
(104) Daskalakis, V.; Farantos, S. C.; Varotsis, C. *J. Am. Chem. Soc.* **2008**, *130*, 12385–12393.
(105) Iachello, F.; Perez-Bernal, F. *Mol. Phys.* **2008**, *106*, 223–231.
(106) Tabor, M. *Chaos and Integrability in Nonlinear Mechanics*, 1st ed.; John Wiley & Sons Inc.: New York, 1989.
(107) Kellman, M. E. *J. Chem. Phys.* **1990**, *93*, 6630–6635.
(108) Fried, L. E.; Ezra, G. S. *J. Chem. Phys.* **1987**, *86*, 6270–6282.
(109) Bacic, Z.; Light, J. C. *Annu. Rev. Phys. Chem.* **1989**, *40*, 469–498.
(110) Fornberg, B. *A Practical Guide to Pseudospectral Methods*; Cambridge University Press: Cambridge in Applied and Computational Mathematics, 1998.
(111) Kosloff, R. *Dynamics of Molecules and Chemical Reactions*; Wyatt, R. E., Zhang, J. Z. H., Eds.; New York, 1996.
(112) Guantes, R.; Farantos, S. C. *J. Chem. Phys.* **1999**, *111*, 10827–10835.
(113) Guantes, R.; Farantos, S. C. *J. Chem. Phys.* **2000**, *113*, 10429–10437.
(114) Gray, S. K.; Goldfield, E. M. *J. Chem. Phys.* **2001**, *115*, 8331–8344.
(115) Goldfield, E. M. *Comput. Phys. Commun.* **2000**, *128*, 178–189.
(116) Goldfield, E. M.; Gray, A. K. *Comput. Phys. Commun.* **1996**, *98*, 1–14.
(117) Medvedev, D. M.; Goldfield, E. M.; Gray, A. K. *Comput. Phys. Commun.* **2005**, *166*, 94–108.
(118) Suarez, J.; Farantos, S. C.; Stamatiadis, S.; Lathouwers, L. Comput. Phys. Commun., in press.
(119) Kosloff, R. *Annu. Rev. Phys. Chem.* **1994**, *45*, 145–178.
(120) Wall, M. R.; Neuhauser, D. *J. Chem. Phys.* **1995**, *102*, 8011–8022.
(121) Mandelshtam, V. A.; Taylor, H. S. *J. Chem. Phys.* **1995**, *102*, 7390–7399.
(122) Chen, R.; Guo, H. *J. Chem. Phys.* **1996**, *105*, 1311–1317.
(123) Mandelshtam, V. A.; Grozdanov, T. P.; Taylor, H. S. *J. Chem. Phys.* **1995**, *103*, 10074–10084.
(124) Mandelshtam, V. A.; Taylor, H. S. *J. Chem. Soc., Faraday Trans.* **1997**, *93*, 847–860.
(125) Carrington, T., Jr. *Can. J. Chem.* **2004**, *82*, 900–914.
(126) Guo, H. *Rev. Comput. Chem.* **2007**, *25*, 285–347.
(127) Golub, G. H.; Loan, V. *Matrix Computations*, 3rd ed.; The Johns Hopkins University Press: Baltimore, MD, 1996.
(128) Lanczos, C. *J. Res. Natl. Bur. Stand.* **1950**, *45*, 255.
(129) Guo, H.; Chen, R.; Xie, D. *J. Theor. Comput. Chem.* **2002**, *1*, 173–185.
(130) Parlett, B. N. *The Symmetric Eigenvalue Problem*; Prentice Hall: Englewood Cliffs, NJ, 1980.
(131) Wyatt, R. E. *Adv. Chem. Phys.* **1989**, *73*, 231–278.
(132) Chen, R.; Guo, H. *J. Chem. Phys.* **1999**, *111*, 9944–9951.
(133) Azzam, T.; Schinke, R.; Farantos, S. C.; Joyeux, M.; Peterson, K. A. *J. Chem. Phys.* **2003**, *118*, 9643–9652.
(134) Jung, C.; Taylor, H. S.; Atilgan, E. *J. Phys. Chem. A* **2002**, *106*, 3092–3101.
(135) Jung, C.; Taylor, H. S.; Sibert, E. L. *J. Phys. Chem. A* **2006**, *110*, 5317–5325.
(136) Keshavamurthy, S. *J. Phys. Chem. A* **2001**, *105*, 2668–2676.
(137) Semparithi, A.; Charaulatha, V.; Keshavamurthy, S. *J. Chem. Phys.* **2003**, *118*, 1146–1157.
(138) Semparithi, A.; Keshavamurthy, S. *Phys. Chem. Chem. Phys.* **2003**, *5*, 5051–5062.
(139) Semparithi, A.; Keshavamurthy, S. *Chem. Phys. Lett.* **2004**, *395*, 327–334.
(140) Laskar, J. *Physica D* **1993**, *67*, 257–281.
(141) von Milczewski, J.; Uzer, T. *Modern Methods for Multidimensional Dynamics Computations in Chemistry*; Singapore, 1998; pp 190−200.
(142) Safi, S. Z.; Losada, J. C.; Benito, R. M.; Borondo, F. *J. Chem. Phys.* **2008**, *129*, 164316.
(143) Losada, J. C.; Benito, R. M.; Borondo, F. *Eur. Phys. J.−Spec. Top.* **2008**, *165*, 183–193.
(144) Vela-Arevalo, L. V.; Wiggins, S. *Int. J. Bifurcation Chaos* **2001**, *11*, 1359–1380.
(145) Chandre, C.; Wiggins, S.; Uzer, T. *Physica D* **2003**, *181*, 171–196.
(146) Crawford, J. D. *Rev. Mod. Phys.* **1991**, *63*, 991–1037.
(147) Farantos, S. C.; Qu, Z.; Zhu, H.; Schinke, R. *Int. J. Bifurcation Chaos Appl. Sci. Eng.* **2006**, *16*, 1913–1928.
(148) Founargiotakis, M.; Farantos, S. C.; Contopoulos, G.; Polymilis, C. *J. Chem. Phys.* **1989**, *91*, 1389–1402.
(149) Contopoulos, G.; Farantos, S. C.; Papadaki, H.; Polymilis, C. *Phys. Rev. E* **1994**, *50*, 4399–4403.
(150) Arnold, V. I. *Mathematical Methods of Classical Mechanics*, 2nd ed.; Springer-Verlag: New York, 1980.
(151) Scheck, F. *Mechanics*, 1st ed.; Springer-Verlag: Berlin, Heidelberg, 1990.
(152) Lichtenberg, A. J.; Liberman, M. A. *Regular and Chaotic Dynamics*, 2nd ed.; Springer: Berlin, 1992.
(153) Birkhoff, G. D. *Trans. Am. Math. Soc.* **1913**, *14*, 14–22.
(154) Gaspard, P.; Burghardt, I. *Adv. Chem. Phys.* **1997**, *101*, 491–621.
(155) Yakubovich, V. A.; Starzhinskii, V. M. *Linear Differential Equations With Periodic Coefficients*; Krieger: Malabar, FL, 1975.
(156) Farantos, S. C. Chemical Dynamics: A Periodic Orbits Approach. In *Time Dependent Quantum Mechanics: Experiments and Theory*; Broeckhove, J., Lathouwers, L., Eds.; 1992; pp 7−43.
(157) Allgower, E. L.; Georg, K. Numerical Continuation Methods; *Springer series in computational mathematics*; Springer-Verlag: Berlin, 1993; Vol. 13.
(158) van der Meer, J.-C. *The Hamiltonian Hopf Bifurcation*; Springer-Verlag: New York, 1985.
(159) Seydel, R. *From Equilibrium to Chaos: Practical bifurcation and stability analysis*; Elsevier: 1988.
(160) Reithmeier, E. Periodic Solutions of Nonlinear Dynamical Systems; *Lecture Notes in Mathematics*; Springer-Verlag: 1991.
(161) Stoer, J.; Bulirsch, R. *Introduction to Numerical Analysis*; Springer: New York, 1980.
(162) Farantos, S. C. *Comput. Phys. Commun.* **1998**, *108*, 240–258.
(163) Stamatiadis, S.; Prosmiti, R.; Farantos, S. C. *Comput. Phys. Commun.* **2000**, *127*, 343–355.
(164) Vrahatis, M. N. *J. Comput. Phys.* **1995**, *119*, 105–119.
(165) Vrahatis, M. N.; Perdiou, A. E.; Kalantonis, V. S.; Perdios, E. A.; Papadakis, K.; Prosmiti, R.; Farantos, S. C. *Comput. Phys. Commun.* **2001**, *138*, 53–68.
(166) Davis, M. J. *Int. Rev. Phys. Chem.* **1995**, *14*, 15–66.
(167) Guantes, R.; Nezis, A.; Farantos, S. C. *J. Chem. Phys.* **1999**, *111*, 10836–10842.
(168) Bhatia, P.; Maiti, B.; Sathyamurthy, N.; Stamatiadis, S.; Farantos, S. C. *Phys. Chem. Chem. Phys.* **1999**, *1*, 1105–1113.
(169) Maiti, B.; Sathyamurthy, N.; Stamatiadis, S.; Farantos, S. C. *Indian J. Chem. A* **2000**, *39A*, 338–344.
(170) Founargiotakis, M.; Farantos, S. C.; Skokos, H.; Contopoulos, G. *Chem. Phys. Lett.* **1997**, *277*, 456–464.
(171) Farantos, S. C. *Laser Chem.* **1993**, *13*, 87–99.
(172) Farantos, S. C.; Lin, S. Y.; Guo, H. *Chem. Phys. Lett.* **2004**, *399*, 260–265.
(173) Lin, S. Y.; Guo, H.; Farantos, S. C. *J. Chem. Phys.* **2005**, *122*, 124308–11.
(174) Banares, L.; Aoiz, F. J.; Vázquez, S. A.; Ho, T.-S.; Rabitz, H. *Chem. Phys. Lett.* **2003**, *374*, 243–251.
(175) Bussery-Honvault, B.; Honvault, P.; Launay, J.-M. *J. Chem. Phys.* **2001**, *115*, 10701–10708.
(176) Weinstein, A. *Inv. Math.* **1973**, *20*, 47–57.
(177) Moser, J. *Commun. Pure Appl. Math.* **1976**, *29*, 727–747.
(178) Kopidakis, G.; Aubry, S. *Physica D* **1999**, *130*, 155–309.
(179) The two symmetric C_{2v} minima of methylene are distinct only on the plane, and they are rotated into one another when rotations are allowed.
(180) Haller, E.; Koppel, H.; Cederbaum, L. S. *Chem. Phys. Lett.* **1983**, *101*, 215–220.
(181) Wigner, E. P. *SIAM Rev.* **1967**, *9*, 1–23.
(182) Dyson, F. J.; Mehta, M. L. *J. Math. Phys.* **1963**, *4*, 701–712.
(183) Green, W. H.; Handy, N. C.; Knowles, P. J.; Carter, S. *J. Chem. Phys.* **1991**, *94*, 118–132.
(184) Jacobson, M. P.; Child, M. S. *J. Chem. Phys.* **2001**, *114*, 250–261.
(185) Jacobson, M. P.; Child, M. S. *J. Chem. Phys.* **2001**, *114*, 262–275.

(186) Newhouse, S. E. *Publ. Math. IHES* **1979**, *50*, 101–151.
(187) Borondo, F.; Zembekov, A. A.; Benito, R. M. *J. Chem. Phys.* **1996**, *105*, 5068–5081.
(188) Yang, S.; Tyng, V.; Kellman, M. E. *J. Phys. Chem. A* **2003**, *107*, 8345–8354.
(189) Porter, C. E.; Thomas, R. G. *Phys. Rev.* **1956**, *104*, 483–491.
(190) Baer, T.; Hase, W. L. *Unimolecular Reaction Dynamics, Theory and Experiments*; Oxford University Press: New York, 1996.
(191) Quack, M.; Troe, J. *Ber. Bunsen-Ges. Phys. Chem.* **1974**, *78*, 240–252.
(192) Xu, C.; Jiang, B.; Xie, D.; Farantos, S. C.; Lin, S. Y.; Guo, H. *J. Phys. Chem. A* **2007**, *111* (41), 10353–10361.
(193) Lin, S. Y.; Xie, D.; Guo, H. *J. Chem. Phys.* **2006**, *125*, 091103.
(194) Ivanov, M. V.; Grebenshchikov, S. Y.; Schinke, R. *J. Chem. Phys.* **2004**, *120*, 10015–10024.
(195) Mauersberger, K.; Erbacher, B.; Krankowsky, D.; Günther, J.; Nickel, R. *Science* **1999**, *283*, 370–372.
(196) Thiemens, M. H. *Science* **2001**, *293*, 226.
(197) Gao, Y. Q.; Marcus, R. A. *Science* **2001**, *293*, 259–263.
(198) Janssen, C.; Marcus, R. A. *Science* **2001**, *294*, 951.
(199) Mauersberger, K.; Krankowsky, D.; Janssen, C.; Schinke, R. *Adv. At. Mol. Opt. Phys.* **2005**, *50*, 1–54.
(200) Janssen, C.; Guenther, J.; Mauersberger, K.; Krankowsky, D. *Phys. Chem. Chem. Phys.* **2001**, *3*, 4718–4721.
(201) Schinke, R.; Fleurat-Lessard, P. *J. Chem. Phys.* **2005**, *122*, 094317.
(202) Schinke, R.; Grebenshchikov, S. Y.; Ivanov, M. V.; Fleurat-Lessard, P. *Annu. Rev. Phys. Chem.* **2006**, *57*, 625–661.
(203) Hathorn, B. C.; Marcus, R. A. *J. Chem. Phys.* **1999**, *111*, 4087–4100.
(204) Hathorn, B. C.; Marcus, R. A. *J. Chem. Phys.* **2000**, *113*, 9497–9509.
(205) Miklovc, A.; Peyrimhoff, S. D. *Chem. Phys. Lett.* **2001**, *359*, 55–62.
(206) Fleurat-Lessard, P.; Grebenshchikov, S. Y.; Siebert, R.; Schinke, R.; Halberstadt, N. *J. Chem. Phys.* **2003**, *118*, 610–621.
(207) Houston, P. L. In Modern Trends in Chemical Dynamics; *Advanced Series in Physical Chemistry*; Liu, K., Yang, X., Ed.; World Scientific: Singapore, 2004; Vol. 14 (part II), p 281.
(208) Grebenshchikov, S. Y.; Qu, Z.; Zhu, H.; Schinke, R. *Phys. Chem. Chem. Phys.* **2007**, *9*, 2044–2060.
(209) Grozdanov, T. P.; Mandelshtam, V. A.; Taylor, H. S. *J. Chem. Phys.* **1995**, *103*, 7990–7995.
(210) Mandelshtam, V. A.; Taylor, H. S. *J. Chem. Phys.* **1997**, *106*, 5085–5090.
(211) Ervin, K. M.; Ho, J.; Lineberger, W. C. *J. Chem. Phys.* **1989**, *91*, 5974–5992.
(212) Bramley, M. J.; Handy, N. C. *J. Chem. Phys.* **1993**, *98*, 1378–1397.
(213) Xu, D.; Li, G.; Xie, D.; Guo, H. *Chem. Phys. Lett.* **2002**, *365*, 480–486.
(214) Xu, D.; Chen, R.; Guo, H. *J. Chem. Phys.* **2003**, *118*, 7273–7282.
(215) Zou, S.; Bowman, J. M. *J. Chem. Phys.* **2002**, *116*, 6667–6673.
(216) Stanton, J. F.; Gauss, J. *J. Chem. Phys.* **1999**, *110*, 1831–1832.
(217) Stanton, J. F.; Gauss, J. *J. Chem. Phys.* **1999**, *110*, 6079–6080.
(218) Carter, S.; Mills, I. M.; Murrell, J. N. *Mol. Phys.* **1980**, *41*, 191–203.
(219) Tremblay, J. C.; Carrington, T., Jr. *J. Chem. Phys.* **2006**, *125*, 094311.
(220) Lin, B.; Bian, W. *J. Chem. Phys.* **2008**, *129*, 024111.
(221) Jacobson, M. P.; Jung, C.; Taylor, H. S.; Field, R. W. *J. Chem. Phys.* **1999**, *111*, 600–618.
(222) Yu, J.; Wu, G. *J. Chem. Phys.* **2000**, *113*, 647–652.
(223) Xu, D.; Guo, H.; Zou, S.; Bowman, J. M. *Chem. Phys. Lett.* **2003**, *377*, 582–588.
(224) Tyng, V.; Kellman, M. E. *J. Phys. Chem. B* **2006**, *110*, 18859–18871.
(225) Bigqood, R.; Millan, B.; Gruebele, M. *Chem. Phys. Lett.* **1998**, *287*, 333–341.
(226) Chowdary, P. D.; Gruebele, M. *J. Chem. Phys.* **2009**, *130*, 134310–8.
(227) Bolhuis, P. G.; Dellago, C.; Chandler, D. *Proc. Natl. Acad. Sci. U.S.A.* **2000**, *97*, 5877–5882.
(228) Ren, W.; Vanden-Eijnden, E.; Maragakis, P.; Weinani, E. *J. Chem. Phys.* **2005**, *123*, 134109–12.
(229) Han, W.-G.; Jalkanen, K. J.; Elstner, M.; Suhai, S. *J. Phys. Chem. B* **1998**, *102*, 2587–2602.
(230) Drozdov, A. N.; Grossfield, A.; Pappu, R. V. *J. Am. Chem. Soc.* **2004**, *126*, 2574–2581.
(231) Farantos, S. C. *CPS-IEEE Comput. Soc.* **2007**, 444–450.
(232) Xie, A.; van der Meer, L.; Hoff, W.; Austin, R. H. *Phys. Rev. Lett.* **2000**, *84*, 5435–5438.
(233) Gruebele, M. *Annu. Rev. Phys. Chem.* **1999**, *50*, 485–516.
(234) Gruebele, M. *Adv. Chem. Phys.* **2000**, *5F1*, 193.
(235) Woutersen, S.; Mu, Y. G. S.; Hamm, P. *Proc. Natl. Acad. Sci. U.S.A.* **2001**, *98*, 11254–11258.
(236) Herman, M.; Lievin, J.; Auwera, J. V.; Campargue, A. *Adv. Chem. Phys.* **1999**, *108*, 1–431.
(237) Fermi, E.; Pasta, J.; Ulam, S. Document LA-1940, May 1955, 978−988.
(238) Ford, J. *Phys. Rep.* **1992**, *213*, 271–310.
(239) Campbell, D. K.; Rosenau, P.; Zaslavsky, G. M. *Chaos* **2005**, *15*, 015101−015121.
(240) Huang, S.; Chandre, C.; Uzer, T. *J. Chem. Phys.* **2008**, *128*, 174105.
(241) Li, C.; Toda, M.; Komatsuzaki, T. *J. Chem. Phys.* **2009**, *130*, 124116–7.
(242) Keshavamurthy, S. *Int. Rev. Phys. Chem.* **2007**, *26*, 521–584.

CR900069M